Fraunhofer
ITWM

N. Marheineke, R. Wegener

Modeling and validation of a stochastic drag for fibers in turbulent flows

Berichte des Fraunhofer ITWM, Nr. 172 (2009)

ISSN 1434-9973

Bericht 172 (2009)

Die Veröffentlichungen in der Berichtsreihe des Fraunhofer ITWM können bezogen werden über:

Fraunhofer-Institut für Techno- und
Wirtschaftsmathematik ITWM
Fraunhofer-Platz 1

67663 Kaiserslautern
Germany

Telefon: +49(0)631/31600-0
Telefax: +49(0)631/31600-1099
E-Mail: info@itwm.fraunhofer.de
Internet: www.itwm.fraunhofer.de

Vorwort

Das Tätigkeitsfeld des Fraunhofer-Instituts für Techno- und Wirtschaftsmathematik ITWM umfasst anwendungsnahe Grundlagenforschung, angewandte Forschung sowie Beratung und kundenspezifische Lösungen auf allen Gebieten, die für Techno- und Wirtschaftsmathematik bedeutsam sind.

In der Reihe »Berichte des Fraunhofer ITWM« soll die Arbeit des Instituts kontinuierlich einer interessierten Öffentlichkeit in Industrie, Wirtschaft und Wissenschaft vorgestellt werden. Durch die enge Verzahnung mit dem Fachbereich Mathematik der Universität Kaiserslautern sowie durch zahlreiche Kooperationen mit internationalen Institutionen und Hochschulen in den Bereichen Ausbildung und Forschung ist ein großes Potenzial für Forschungsberichte vorhanden. In die Berichtreihe sollen sowohl hervorragende Diplom- und Projektarbeiten und Dissertationen als auch Forschungsberichte der Institutsmitarbeiter und Institutsgäste zu aktuellen Fragen der Techno- und Wirtschaftsmathematik aufgenommen werden.

Darüber hinaus bietet die Reihe ein Forum für die Berichterstattung über die zahlreichen Kooperationsprojekte des Instituts mit Partnern aus Industrie und Wirtschaft.

Berichterstattung heißt hier Dokumentation des Transfers aktueller Ergebnisse aus mathematischer Forschungs- und Entwicklungsarbeit in industrielle Anwendungen und Softwareprodukte – und umgekehrt, denn Probleme der Praxis generieren neue interessante mathematische Fragestellungen.

Prof. Dr. Dieter Prätzel-Wolters
Institutsleiter

Kaiserslautern, im Juni 2001

MODELING AND VALIDATION OF A STOCHASTIC DRAG FOR FIBERS IN TURBULENT FLOWS

NICOLE MARHEINEKE AND RAIMUND WEGENER

Abstract. Considering the dynamics of long slender elastic fibers in turbulent flows, a stochastic aerodynamic force concept for a general drag model was derived on the basis of a k-ϵ turbulence description in [23]. In this paper we generalize the concept and formulate an air drag model that is uniformly valid for all Reynolds number regimes and incident flow directions. The associated turbulent force overcomes the hitherto existing limitations and allows the simulation of all kind of fibers (flexible, stiff, light, heavy) immersed in turbulent flows. Moreover, the validation of the numerical results with PIV-measurements shows very convincing agreements in the industrial application of technical textile manufacturing.

Key words. fiber-fluid interactions, long slender fibers, turbulence modelling, aerodynamic drag, dimensional analysis, data interpolation, stochastic partial differential algebraic equation, numerical simulations, experimental validations

1. Introduction

The understanding of the motion of long slender elastic fibers in turbulent flows is of great interest to research, development and production in technical textiles manufacturing. The fiber dynamics depend on the drag forces that are imposed on the fiber by the fluid. Their computation requires in principle a coupling of fiber and flow with no-slip interface conditions. However, the needed high resolution and adaptive grid refinement make the direct numerical simulation of the three-dimensional fluid-solid-problem for slender fibers and turbulent flows not only extremely costly and complex, but also still impossible for practically relevant applications. Embedded in a slender body theory, an aerodynamic force concept for a general drag model was therefore derived on basis of a stochastic k-ϵ description for a turbulent flow field in [23]. The turbulence effects on the fiber dynamics were modeled by a correlated random Gaussian force and its asymptotic limit on a macroscopic fiber scale by Gaussian white noise with flow-dependent amplitude. The concept was numerically studied under the conditions of a melt-spinning process for nonwoven materials in [24] – for the specific choice of a non-linear Taylor drag model. Taylor [35] suggested the heuristic model for high Reynolds number flows, $\mathrm{Re} \in [20, 3 \cdot 10^5]$, around inclined slender objects under an angle of attack of $\alpha \in (\pi/36, \pi/2]$ between flow and object tangent. Since the Reynolds number is considered with respect to the relative velocity between flow and fiber, the numerical results lack accuracy evidently for small Re that occur in cases of flexible light fibers moving occasionally with the flow velocity. In such a regime ($\mathrm{Re} \ll 1$), linear Stokes drag forces were successfully applied for the prediction of small particles immersed in turbulent flows, see e.g. [25, 26, 32, 39], a modified Stokes force taking also into account the particle oscillations was presented in [14]. The linear drag relation was also conferred to longer filaments by imposing free-draining assumptions [29, 8]. Apart from this, the Taylor drag suffers from its non-applicability to tangential incident flow situations ($\alpha = 0$) that often occur in fiber and nonwoven production processes.

The goal of our paper is the generalization of the stochastic aerodynamic force context and the formulation of a drag model that is uniformly valid for all Reynolds number regimes and incident flow directions. The associated turbulent force overcomes then the observed limitations and allows the efficient simulation of all variants of long slender fibers (i.e. flexible, stiff, light, heavy) immersed in turbulent flows.

Date: August 20, 2009.

For convenience, we start with a brief outline of the aerodynamic force concept [23] that is based on a splitting of the instantaneous force into a mean and a fluctuating part in Section 1. The mean force model as well as the splitting approach require an appropriate air drag model that is valid for all Reynolds number regimes and incident flow directions. Motivated from Oseen and Stokes slender body theories for small Re (see e.g. [20, 36, 37, 18, 27, 16, 5] for Oseen and [6, 3, 19, 2, 13] for Stokes flow), empirical drag models for high Re [35, 17] and measurements [38, 31, 30, 33], we formulate a continuously differentiable drag that we verify by help of simulations in Section 2. In Section 3 we suggest a splitting approach that reduces to a linearization of the drag model for small turbulent kinetic energy $\mathrm{k} \to 0$. The fluctuation force is asymptotically modelled by Gaussian white noise with flow-dependent amplitude. The amplitude is thereby deduced from the correlations of the turbulent flow velocity. Following [23], the double-velocity correlation tensor of the assumed centered differentiable Gaussian field satisfies initially the Kolmogorov universal equilibrium theory [10] as well as the local distribution of the kinetic energy k and dissipation rate ϵ provided by the stochastic k-ϵ turbulence model. We weaken Taylor's hypothesis of frozen turbulence pattern [34] originally proposed in [23] and incorporated in [24] by prescribing a dynamic decay of the local correlations in Section 4. This modification extends the applicability range of the stochastic force model crucially. Tangential incident as well as low Reynolds number flow scenarios are included as the numerical simulations of fiber-turbulence interactions in melt-spinning processes of nonwoven materials show in Section 5. We conclude this work with the validation of our proposed stochastic drag model with PIV-measurements.

General Stochastic Aerodynamic Force Concept. Being interested in the dynamics of long slender fibers in turbulent flows, we briefly recall the basic models developed in [23].

Consider a single elastic fiber of slenderness ratio $\delta = \mathrm{d}/\mathrm{l} \ll 1$ with length l and circular cross-sections of typical diameter d that is immersed in a subsonic highly turbulent air flow with small pressure gradients and Mach number $\mathrm{Ma} < 1/3$. Its motion is crucially affected by the aerodynamic force, i.e. the stress on the fiber boundary in outer normal direction. The determination of the aerodynamic force requires in principle a two-way coupling of fiber and flow with no-slip interface conditions. In case of slender fibers and turbulent flows, the needed high resolution and adaptive grid refinement make the direct numerical simulation of the coupled fluid-solid-problem not only extremely costly and complex, but also still impossible for practically relevant applications. Since the fiber influence on the turbulence is negligibly small due to the slender geometry, it makes therefore sense to associate to the force a stochastic drag that characterizes the turbulent flow effects on the fiber and allows an one-way coupling. Representing the fiber as arc-length parameterized time-dependent curve $\mathbf{r} : [0,\mathrm{l}] \times \mathbb{R}_0^+ \to \mathbb{R}^3$ with line weight $(\rho\mathrm{A})$, its motion is asymptotically modeled by a system of stochastic partial differential equations with algebraic constraint of inextensibility, i.e.,

$$\|\partial_\mathrm{s}\mathbf{r}\|_2 = 1 \tag{1.1a}$$

$$(\rho\mathrm{A})\,\partial_{\mathrm{tt}}\mathbf{r}\,\mathrm{ds}\,\mathrm{dt} = \{\,\partial_\mathrm{s}(\mathrm{T}\,\partial_\mathrm{s}\mathbf{r} - \partial_\mathrm{s}(\mathrm{EI}\,\partial_{\mathrm{ss}}\mathbf{r})) + (\rho\mathrm{A})\,\mathbf{g} + \mathbf{a}(\mathbf{r}, \partial_\mathrm{t}\mathbf{r}, \partial_\mathrm{s}\mathbf{r}, \mathrm{s}, \mathrm{t})\,\}\,\mathrm{ds}\,\mathrm{dt} + \mathbf{A}(\mathbf{r}, \partial_\mathrm{t}\mathbf{r}, \partial_\mathrm{s}\mathbf{r}, \mathrm{s}, \mathrm{t}) \cdot \mathrm{d}\mathbf{w}_{\mathrm{s,t}} \tag{1.1b}$$

equipped with appropriate initial and boundary conditions, where

$$\mathbf{a}(\mathbf{x}, \mathbf{w}, \boldsymbol{\tau}, \mathrm{s}, \mathrm{t}) = \mathbf{m}(\boldsymbol{\tau}, \bar{\mathbf{u}}(\mathbf{x}, \mathrm{t}) - \mathbf{w}, \mathrm{k}(\mathbf{x}, \mathrm{t}), \nu(\mathbf{x}, \mathrm{t}), \rho(\mathbf{x}, \mathrm{t}), \mathrm{d}(\mathrm{s})), \tag{1.1c}$$

$$\mathbf{A}(\mathbf{x}, \mathbf{w}, \boldsymbol{\tau}, \mathrm{s}, \mathrm{t}) = \mathbf{L}(\boldsymbol{\tau}, \bar{\mathbf{u}}(\mathbf{x}, \mathrm{t}) - \mathbf{w}, \mathrm{k}(\mathbf{x}, \mathrm{t}), \nu(\mathbf{x}, \mathrm{t}), \rho(\mathbf{x}, \mathrm{t}), \mathrm{d}(\mathrm{s})) \cdot \mathbf{D}(\boldsymbol{\tau}, \bar{\mathbf{u}}(\mathbf{x}, \mathrm{t}) - \mathbf{w}, \mathrm{k}(\mathbf{x}, \mathrm{t}), \epsilon(\mathbf{x}, \mathrm{t}), \nu(\mathbf{x}, \mathrm{t})). \tag{1.1d}$$

The system is deduced from the dynamical Kirchhoff-Love equations [1] for a Cosserat rod being capable of large, geometrically nonlinear deformations, neglecting torsion. In (1.1b) the change of the momentum is balanced by the acting internal and external forces. The internal line forces stem from bending stiffness indicated by Young's modulus and the moment of inertia (EI) as well as from traction. In this spirit, the Lagrangian multiplier $\mathrm{T} : [0,\mathrm{l}] \times \mathbb{R}_0^+ \to \mathbb{R}$ to (1.1a) can be viewed as modified tractive force $\mathrm{T} = \mathrm{T_t} + \mathrm{EI}\,\|\partial_{\mathrm{ss}}\mathbf{r}\|_2^2$ containing tension $\mathrm{T_t}$ and curvature $\|\partial_{\mathrm{ss}}\mathbf{r}\|_2^2$ due to bending. The external line forces imposed on the fiber arise from gravity $\mathbf{g}$ and aerodynamics $\mathbf{a}$, $\mathbf{A}$.

The aerodynamic force is derived on basis of a stochastic k-ϵ turbulence model [21]. Expressing the instantaneous flow velocity as sum of a mean and a fluctuating part, the Reynolds-averaged Navier-Stokes equations (RANS) yield a deterministic description for the mean velocity $\bar{\mathbf{u}} : \mathbb{R}^3 \times \mathbb{R}_0^+ \to \mathbb{R}^3$, whereas two further transport equations for the kinetic turbulent energy $\mathrm{k} : \mathbb{R}^3 \times \mathbb{R}_0^+ \to \mathbb{R}^+$ and dissipation rate $\epsilon : \mathbb{R}^3 \times \mathbb{R}_0^+ \to \mathbb{R}^+$ characterize the random fluctuations $\mathbf{u}'$ according to $\mathrm{k} = \mathbb{E}[\mathbf{u}' \cdot \mathbf{u}']/2$ and $\epsilon = \nu\,\mathbb{E}[\nabla\mathbf{u}' : \mathbf{u}']$ with kinematic viscosity ν, density ρ and expectation $\mathbb{E}[.]$. Analogously, the aerodynamic force is split into a mean and a fluctuating part. Acting as additive Gaussian noise in (1.1b), it depends on the flow quantities $\bar{\mathbf{u}}$, k, ϵ, and ν, ρ, cf. (1.1c), (1.1d). Thereby, the deterministic mean force $\mathbf{m} : \mathbb{R}^2 \times \mathbb{R}^3 \times (\mathbb{R}^+)^4 \to \mathbb{R}^3$ as well as the associated splitting operator $\mathbf{L} : \mathbb{R}^2 \times \mathbb{R}^3 \times (\mathbb{R}^+)^4 \to \mathbb{R}^{3\times 3}$ are determined by the chosen air drag model $\mathbf{f}$ which is a function of the mean relative velocity between fluid and fiber, $\bar{\mathbf{u}}(\mathbf{r}, \mathrm{t}) - \partial_{\mathrm{t}}\mathbf{r}$, and the fiber tangent $\partial_{\mathrm{s}}\mathbf{r}$. The correlated fluctuations are asymptotically approximated by Gaussian white noise with turbulence-dependent amplitude, where $(\mathbf{w}_{\mathrm{s,t}}, (\mathrm{s}, \mathrm{t}) \in [0, \mathrm{l}] \times \mathbb{R}_0^+)$ denotes a $\mathbb{R}^3$-valued Wiener process (Brownian motion). The amplitude $\mathbf{D} : \mathbb{R}^2 \times \mathbb{R}^3 \times (\mathbb{R}^+)^3 \to \mathbb{R}^{3\times 3}$ represents the integral effects of the localized centered Gaussian velocity fluctuations on the relevant fiber scales by containing the necessary information of the spatial and temporal correlations of the double-velocity fluctuations $\boldsymbol{\gamma} = \mathbb{E}[\mathbf{u}' \otimes \mathbf{u}']$.

Consequently, the performance of the aerodynamic force mainly relies on two models, i.e. the air drag model $\mathbf{f}$ (inducing $\mathbf{m}$ and $\mathbf{L}$) and the turbulence correlation approximation $\boldsymbol{\gamma}$ (inducing $\mathbf{D}$). Applying the Global-from-Local Concept of [23] we derive local models in the following that we globalize by superposition. Hence, we handle the delicate fiber-turbulence problem by help of two surrogate models: a drag model for an incompressible flow around an inclined infinitely long circular cylinder and a correlation model for incompressible homogeneous isotropic turbulence.

Notational Convention *Note that we typeset dimensional quantities in Roman style (e.g.* s, t, $\mathbf{f}$, $\mathbf{m}$, $\mathbf{L}$, $\mathbf{D}$*) and the corresponding dimensionless quantities in Italic style (e.g.* s, t, $\boldsymbol{f}$, $\boldsymbol{m}$, $\boldsymbol{L}$, $\boldsymbol{D}$*) throughout this paper. Moreover, we use small and large bold-faced letters for vector- and tensor-valued quantities, respectively. Scalar-valued quantities are given in normal-faced letters.*

2. Air Drag Model

The flow around slender objects was subject of research during the last century and intensively studied theoretically, numerically and experimentally, for on overview see [41, 33, 31] and references within. In an incompressible flow, the force $\mathbf{f}$ acting on a fixed, infinitely long circular cylinder is exclusively caused by friction and inertia. It depends on the material and geometrical properties, i.e. fluid density ρ, kinematic viscosity ν and cylinder diameter d, as well as on the specific inflow situation, i.e. inflow velocity $\mathbf{v}$ and cylinder orientation $\boldsymbol{\tau}$, $\|\boldsymbol{\tau}\|_2 = 1$, see Figure 2.1. Non-dimensionalizing the line force $\mathbf{f}$ and the flow velocity $\mathbf{v}$ with the typical mass $\rho\mathrm{d}^3$, length d and time d^2/ν yields a reduction of the dependencies,

$$\mathbf{f}(\boldsymbol{\tau}, \mathbf{v}, \nu, \rho, \mathrm{d}) = \frac{\rho\nu^2}{\mathrm{d}}\,\boldsymbol{f}\left(\boldsymbol{\tau}, \frac{\mathrm{d}}{\nu}\mathbf{v}\right), \qquad \mathbf{v} = \frac{\nu}{\mathrm{d}}\boldsymbol{v}. \tag{2.1}$$

In the following we focus on the derivation of the dimensionless quantity $\boldsymbol{f}(\boldsymbol{\tau}, \boldsymbol{v})$.

2.1. Non-tangential Incident Flow.

For the further discussion, we firstly exclude the tangential incident flow situation and assume $\boldsymbol{v} \not\parallel \boldsymbol{\tau}$. Then, we introduce

$$v_\tau = \boldsymbol{v} \cdot \boldsymbol{\tau}, \quad v_n = \sqrt{\boldsymbol{v}^2 - v_\tau^2}, \quad \boldsymbol{n} = \frac{\boldsymbol{v} - v_\tau\boldsymbol{\tau}}{v_n}, \quad \boldsymbol{b} = \boldsymbol{\tau} \times \boldsymbol{n}$$

such that $(\boldsymbol{n}, \boldsymbol{b}, \boldsymbol{\tau})$ forms an orthonormal basis induced by $(\boldsymbol{\tau}, \boldsymbol{v})$. In this context, the dimensionless normal velocity component v_n is the Reynolds number Re and $v_\tau/v_n = \cot\alpha$ can be associated with the angle of attack α.

Due to the rotational invariance of the force, its components depend only on the scalar products $\boldsymbol{v} \cdot \boldsymbol{\tau}$ and $\boldsymbol{v}^2$ such that we can express them alternatively in the tangential and normal velocity components

$$\boldsymbol{f}(\boldsymbol{\tau}, \boldsymbol{v}) = f_n(v_n, v_\tau)\boldsymbol{n} + f_\tau(v_n, v_\tau)\boldsymbol{\tau}.$$

The binormal force component vanishes in case of a circular cylinder due to symmetry reasons, $f_b(v_n, v_\tau) = 0$, as we will see in the following consideration. For the dependencies of the normal and tangential component, Hoerner [15] postulated an independence principle. Since there can be found a lot of very vague explanations and speculations about this principle in literature, we derive it strictly for a stationary flow around a circular cylinder.

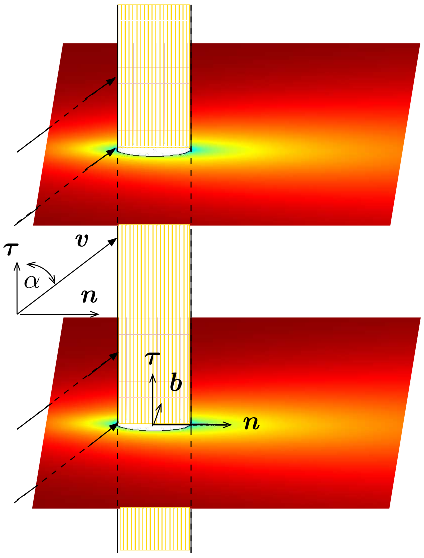

FIGURE 2.1. Flow around infinitely long cylinder with angle of attack α, $\alpha \neq 0$. Inflow set-up yields homogeneous velocity field in $\boldsymbol{\tau}$-direction.

Independence Principle.

- *The normal force f_n is independent of the tangential velocity v_τ.*
- *The tangential force f_τ depends linearly on the tangential velocity v_τ.*

In particular, we formulate

$$f_n(v_n, v_\tau) = v_n^2\, c_n(v_n), \quad f_\tau(v_n, v_\tau) = v_\tau\, v_n\, c_\tau(v_n). \tag{2.2}$$

Proof: With respect to the $(\boldsymbol{n}, \boldsymbol{b}, \boldsymbol{\tau})$-basis, we introduce the tupels $\mathsf{x} = (\mathsf{x}_\perp, x_\tau) = (x_n, x_b, x_\tau)$, $\mathsf{u} = (\mathsf{u}_\perp, u_\tau) = (u_n, u_b, u_\tau)$ and $\mathsf{f} = (\mathsf{f}_\perp, f_\tau) = (f_n, f_b, f_\tau)$ for position, velocity and line force, respectively. Describing a stationary, incompressible flow around a fixed circular cylinder, the three-dimensional Navier-Stokes equations for pressure p and velocity u are

$$\nabla_\mathsf{x} \cdot \mathsf{u} = 0, \qquad \mathsf{u} \cdot \nabla_\mathsf{x} \mathsf{u} = -\nabla_\mathsf{x} p + \triangle_\mathsf{x} \mathsf{u}$$

with inflow velocity $\lim_{x_n \to -\infty} \mathsf{u} = (v_n, 0, v_\tau)$ and no-slip conditions $\mathsf{u} = \mathsf{0}$ at the cylinder.

Note that due to the chosen non-dimensionalization, the parameters characterizing the flow, i.e. Reynolds number $\mathrm{Re} = v_n$ and angle of attack $\alpha = \operatorname{arccot}(v_\tau/v_n)$, occur in the boundary conditions and not in the balance equations themselves. Because of the homogeneity of the flow in $\boldsymbol{\tau}$-direction, i.e. $\partial_{x_\tau} p = 0$, $\partial_{x_\tau} \mathsf{u} = \mathsf{0}$, which is a consequence of the inflow set-up (cf. Figure 2.1), the three-dimensional model decomposes into two-dimensional Navier-Stokes equations for p and $\mathsf{u}_\perp$ and a two-dimensional drift-diffusion equation for u_τ,

$$\nabla_{\mathsf{x}_\perp} \cdot \mathsf{u}_\perp = 0, \qquad \mathsf{u}_\perp \cdot \nabla_{\mathsf{x}_\perp} \mathsf{u}_\perp = -\nabla_{\mathsf{x}_\perp} p + \triangle_{\mathsf{x}_\perp} \mathsf{u}_\perp \qquad\qquad \mathsf{u}_\perp \cdot \nabla_{\mathsf{x}_\perp} u_\tau = \triangle_{\mathsf{x}_\perp} u_\tau \tag{2.3}$$

$$\lim_{x_n \to -\infty} \mathsf{u}_\perp = (v_n, 0) \text{ and } \mathsf{u}_\perp = \mathsf{0} \text{ at the cylinder}, \qquad \lim_{x_n \to -\infty} u_\tau = v_\tau \text{ and } u_\tau = 0 \text{ at the cylinder.}$$

As for the inflow, the flow field $\mathsf{u}_\perp$ depends hence only on the normal component v_n. This dependence is handed over to u_τ due to the one-sided coupling of the equations. Moreover, u_τ depends linearly on v_τ which follows from the linearity of the drift-diffusion equation.

The determination of the line force on the cylinder

$$\mathsf{f} = \int_\gamma -p\tilde{\mathsf{n}} + (\nabla_\mathsf{x} \mathsf{u} + \nabla_\mathsf{x} \mathsf{u}^T) \cdot \tilde{\mathsf{n}}\, \mathrm{d}l,$$

simplifies respectively,

$$\mathsf{f}_\perp = \int_\gamma -p\tilde{\mathsf{n}}_\perp + (\nabla_{\mathsf{x}_\perp}\mathsf{u}_\perp + \nabla_{\mathsf{x}_\perp}\mathsf{u}_\perp{}^T)\cdot\tilde{\mathsf{n}}_\perp \,\mathrm{d}l, \qquad f_\tau = \int_\gamma \tilde{\mathsf{n}}_\perp \cdot \nabla_{\mathsf{x}_\perp} u_\tau \,\mathrm{d}l, \tag{2.4}$$

because of the homogeneity of the flow. Here, the outer normal is given by $\tilde{\mathsf{n}} = (\tilde{\mathsf{n}}_\perp, 0)$ due to the orientation of the cylinder. For a circular cylinder, $\mathsf{f}_\perp = (f_n, 0)$ particularly holds because of symmetry reasons. Since f_n depends exclusively on $\mathsf{u}_\perp$ and f_τ is linear in u_τ, the force inherits the observed dependencies of the flow problem. □

A stationary flow regime around a cylinder develops for small Reynolds numbers, up to approximately $\mathrm{Re} \approx 30$. For higher Reynolds numbers laminar vortex shedding that transits into turbulence in the wake at $\mathrm{Re} \approx 200$ causes a transient flow behavior. However, in the spirit of time-averaged forces, direct numerical simulations (DNS) [22] show the validity of the independence principle even for subcritical Reynolds numbers. Therefore, we apply the principle to all flow regimes. This reduces f_n to the force obtained from cross-flow ($v_\tau = 0$) for all inflow directions, which we express in (2.2) by formulating f_n in terms of the well-studied drag coefficient c_n for cross-flow, see Figure 2.2 as well as [31, 41] and references within. Correspondingly, we introduce a tangential drag coefficient c_τ in (2.2). In contrast to c_n, we lack of theoretical and experimental data for c_τ over a wide range. Since c_n and c_τ play on the same scales, it makes sense to consider

$$c(v_n) = \frac{c_\tau}{c_n}(v_n).$$

A ratio $c(v_n) = 1$ corresponds to a force in direction of the inflow velocity $\boldsymbol{v}$. In general, a smaller tangential force might be expected which promises $c(v_n) \in [0, 1]$ to be a sensitive measure for the modelling of c_τ.

For the scenario of an infinitely long cylinder in cross-flow, Lamb [20] derived c_n by approximating the solution of Oseen flow for $\mathrm{Re} \ll 1$. Among all the extended solutions, see [2, 16, 18, 27] and overview in [41], the exact Oseen drag by Tomotika and Aoi is especially worth mentioning. By help of higher order series expansions in Re with Bessel functions they generalized not only Lamb's result up to $\mathrm{Re} < 4$ [36], but also transfered the techniques to arbitrary inflow directions yielding c_τ in this regime [37]. In Table 2.1 only the first correction to Lamb is listed. For high Reynolds number flows, heuristic drag models for c_n were formulated in correspondence to experimental measurements in cross-flow [38, 31, 30, 33]. Whereas Taylor's model [35] coincides satisfactorily for $\mathrm{Re} \in [20, 3 \cdot 10^5]$, Imai [17] takes into account the drag drop from 0.5 down to 0.25 that is caused by compressibility effects in the critical to transcritical regimes, and pays instead the price of generally underestimating c_n for $\mathrm{Re} \in [10^2, 10^5]$, see Figure 2.2. For the tangential drag, Taylor suggested $c_\tau = \gamma/\sqrt{v_n}$ where the coefficient $\gamma = 2.7$ is adapted to an experiment by Relf et. al., see [35]. To model a trustable tangential drag, we complement the available data by a series of simulations in the moderate Reynolds number regime based on (2.4). The efficient numerical handling of the underlying fluid dynamical problem is thereby allowed by the model reduction from the three-dimensional Navier-Stokes equations to the two-dimensional Navier-Stokes-drift-diffusion equations (2.3). The approximation quality of the performed COMSOL simulations is ensured by the validation with the cross-flow measurements and the Oseen theory, see Figure 2.2. On top of the simulation data, we propose an exponential, continuously differentiable least-square fit to close the gap between Tomotika et. al. and Taylor (cf. Table 2.1). Also the Taylor coefficient γ in c_τ is modified accordingly. This yields the following drag model (2.5), that is uniformly applicable for all Reynolds number regimes and incident flow situations – apart from tangential flow. The respective normal c_n and tangential c_τ components are visualized in Figure 2.3, their ratio c in Figure 2.4.

Flow regime		c_n	c_τ
Flow around infinitely long cylinder			
Oseen drag	low Re		with $S(v_n) = 2.0022 - \ln v_n$
Lamb [20]	$\ll 1$	$\dfrac{4\pi}{Sv_n}$	$\dfrac{4\pi}{(2S-1)v_n}$ *
Tomotika et. al. [36, 37]	< 4	$\dfrac{4\pi}{Sv_n}(1 - \dfrac{S^2 - S/2 + 5/16}{32S} v_n^2)$	$\dfrac{4\pi}{(2S-1)v_n}(1 - \dfrac{2S^2 - 2S + 1}{16(2S-1)} v_n^2)$
Heuristic drag	high Re		
Imai [17]	> 5	$\dfrac{5.85}{v_n} + \dfrac{2.42}{\sqrt{v_n}} + 0.25$	
Taylor [35]	$[20, 3 \cdot 10^5]$	$\dfrac{2}{\sqrt{v_n}} + 0.5$	$\dfrac{2.7}{\sqrt{v_n}}$
Flow around finite cylinder			
Stokes drag	low Re		with $\delta = \mathrm{d/l}$
Cox [6], Batchelor [3]	$\ll 1$	$\dfrac{4\pi}{\ln(4/\delta)v_n}$	$\dfrac{2\pi}{\ln(4/\delta)v_n}$
Götz et. al. [13]	< 1	$\dfrac{4\pi}{(\ln(4/\delta) - 0.5)v_n}$	$\dfrac{2\pi}{(\ln(4/\delta) - 1.5)v_n}$
Keller et. al. [19]	< 1	$\dfrac{4\pi}{(\ln(4/\delta) - 0.5 - \frac{1-\pi^2/12}{\ln(2/\delta)})v_n}$	$\dfrac{2\pi}{(\ln(4/\delta) - 1.5 - \frac{1-\pi^2/12}{\ln(2/\delta)})v_n}$

TABLE 2.1. Selection of existing drag models for respective flow regimes (* c_τ supplemented according to [37])

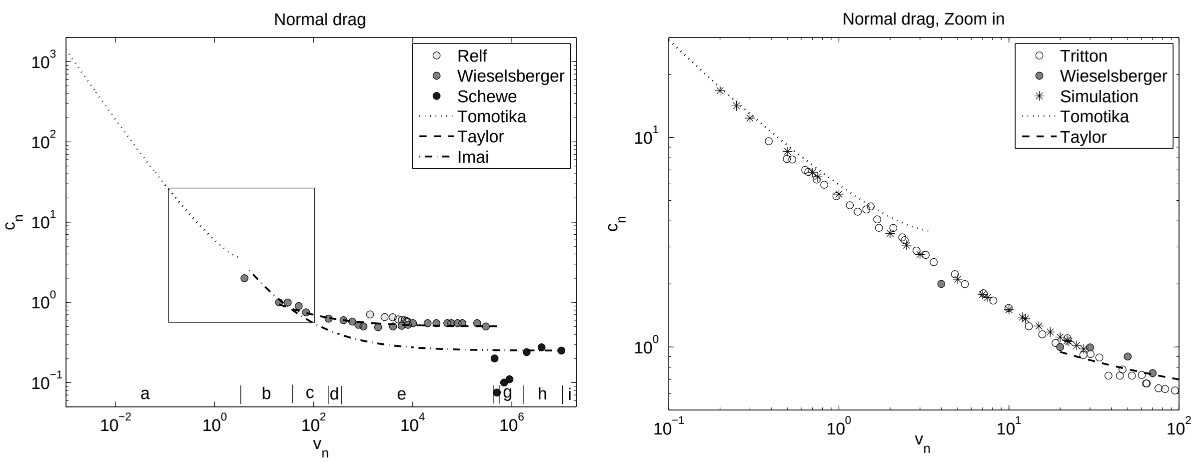

FIGURE 2.2. c_n for a smooth circular cylinder for different flow regimes: a. no vortex separation; b. fixed pair of symmetric vortices; c. laminar vortex separation; d. transition to turbulence in the wake; e. subcritical; f. critical; g. supercritical; h. upper transition; i. transcritical, cf. [33]. Experiments in cross-flow by Tritton [38], Relf et. al (see [35]), Wieselsberger (see [31]), Schewe [30]. Simulations of (2.4) with COMSOL.

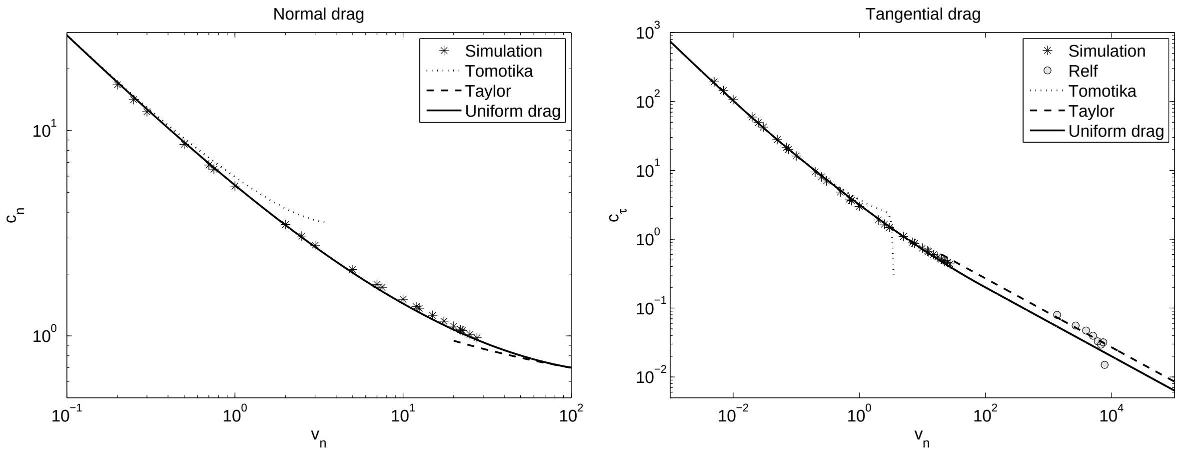

FIGURE 2.3. Normal c_n and tangential c_τ components of proposed uniform drag model (2.5).

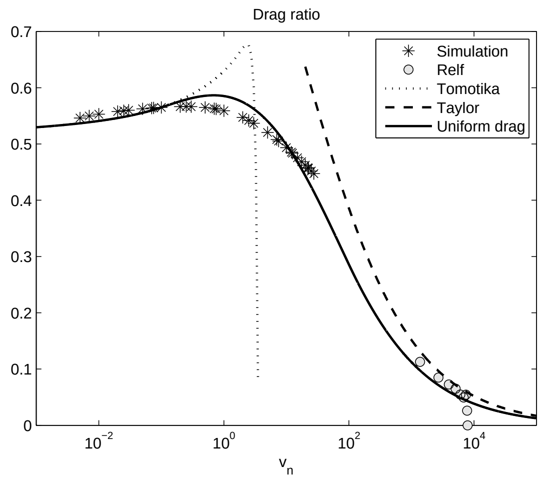

FIGURE 2.4. Drag ratio $c = c_\tau / c_n$.

Uniform Drag Model. *The continuously differentiable normal c_n and tangential c_τ drag models composed of Oseen theory, Taylor heuristic and numerical simulations read*

$$c_n(v_n) = \begin{cases} 4\pi/(Sv_n)\,(1 - \frac{S^2 - S/2 + 5/16}{32S} v_n^2) & v_n < v_1 \\ \exp(\sum_{j=0}^{3} p_{n,j} \ln^j v_n) & v_1 \leq v_n \leq v_2 \\ 2/\sqrt{v_n} + 0.5 & v_2 < v_n \end{cases} \tag{2.5a}$$

$$c_\tau(v_n) = \begin{cases} 4\pi/((2S-1)v_n)\,(1 - \frac{2S^2 - 2S + 1}{16(2S-1)} v_n^2) & v_n < v_1 \\ \exp(\sum_{j=0}^{3} p_{\tau,j} \ln^j v_n) & v_1 \leq v_n \leq v_2 \\ \gamma/\sqrt{v_n} & v_2 < v_n \end{cases} \tag{2.5b}$$

with $S(v_n) = 2.0022 - \ln v_n$. The transition points $v_1 = 0.1$, $v_2 = 100$ as well as the amplitude $\gamma = 2$ are estimated from a least-square approximation of the data. This yields the associated $\mathcal{C}^1$-regularity parameters $p_{n,0} = 1.6911$, $p_{n,1} = -6.7222 \cdot 10^{-1}$, $p_{n,2} = 3.3287 \cdot 10^{-2}$, $p_{n,3} = 3.5015 \cdot 10^{-3}$ and $p_{\tau,0} = 1.1552$, $p_{\tau,1} = -6.8479 \cdot 10^{-1}$, $p_{\tau,2} = 1.4884 \cdot 10^{-2}$, $p_{\tau,3} = 7.4966 \cdot 10^{-4}$.

2.2. **Tangential Incident Flow.** The tangential flow along the cylinder, $\boldsymbol{\tau} \| \boldsymbol{v}$, is a special case that is not included in the previous consideration. Therefore, it is not surprising that the proposed uniform drag model in (2.5) yields an unrealistic force with a vanishing tangential component $\lim_{v_n \to 0} f_\tau(v_n, v_\tau) = 0$. Moreover, the drag force lacks total differentiability on the line $v_n = 0$ due to the symmetric inflow set-up.

To discuss the regularity in more detail, it is reasonable to introduce the resistance coefficients

$$r_n(v_n) = v_n c_n(v_n), \qquad r_\tau(v_n) = v_n c_\tau(v_n). \tag{2.6}$$

associated to (2.5). For a differentiable force, the derivatives of the resistance coefficients must vanish in $v_n = 0$. To obtain such a behavior, we take into account Stokes theory. For slender bodies of finite length (ellipsoids and cylindrical filaments) immersed in slow Stokes flow, appropriate linear force models were asymptotically derived using analytical expansions and matching principles, e.g. [6, 3, 19, 13], Table 2.1. In leading order, Cox [6] and Batchelor [3] particularly found resistance coefficients for $v_n \ll 1$ that depend exclusively on the slenderness ratio δ of the cylinder, $\delta = \mathrm{d}/\mathrm{l} \ll 1$, i.e. $r_{n,C} = 4\pi/\ln(4\delta^{-1})$ and $r_{\tau,C} = 2\pi/\ln(4\delta^{-1})$. Considering a typical slenderness ratio δ as regularization parameter for our drag model, we suggest the following regularization

$$r_n^\delta(v_n) = \begin{cases} \sum_{j=0}^{3} s_{n,j}\, v_n^j, & v_n < v_0 \\ r_n(v_n), & v_0 \le v_n \end{cases}, \qquad r_\tau^\delta(v_n) = \begin{cases} \sum_{j=0}^{3} s_{\tau,j}\, v_n^j, & v_n < v_0 \\ r_\tau(v_n), & v_0 \le v_n \end{cases} \tag{2.7}$$

that matches Stokes resistance coefficients of higher order for $v_n \ll 1$

$$r_{n,S} = \frac{4\pi}{\ln(4/\delta)} - \frac{\pi}{\ln^2(4/\delta)}, \qquad r_{\tau,S} = \frac{2\pi}{\ln(4/\delta)} + \frac{\pi/2}{\ln^2(4/\delta)}. \tag{2.8}$$

to those corresponding to our uniform drag (2.6). The δ-dependence enters (2.7) via the definition of the transition point $v_0 = 2\,(\exp(2.0022) - 4\pi/r_{n,S})$ and the $\mathcal{C}^1$-regularity parameters $s_{i,0} = r_{i,S}$, $s_{i,1} = 0$, $s_{i,2} = (3r_i(v_0) - v_0 r_i'(v_0) - 3r_{i,S})/(v_0)^2$ and $s_{i,3} = (-2r_i(v_0) + v_0 r_i'(v_0) + 2r_{i,S})/(v_0)^3$ for $i = n, \tau$. In order to locate the transition point in the low Reynolds number regime, the condition $v_0 < v_1 = 0.1$ must be fulfilled which implies a restriction on δ, i.e. $\delta < 3.5 \cdot 10^{-2}$. This regularization affects the drag ratio only marginally, but the force essentially, see Figure 2.5. The regularized resistance coefficients (2.7) allow for a smooth force $\boldsymbol{f}$, accordingly

$$\boldsymbol{f}(\boldsymbol{\tau}, \boldsymbol{v}) = v_n\, r_n^\delta(v_n)\, \boldsymbol{n} + v_\tau\, r_\tau^\delta(v_n)\, \boldsymbol{\tau}.$$

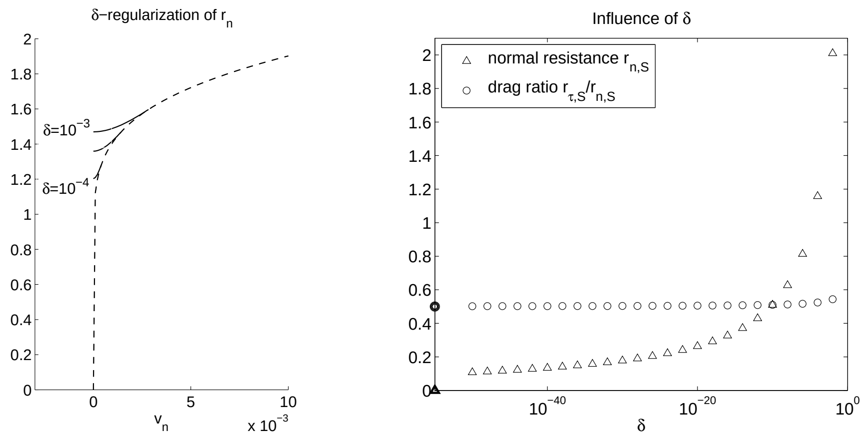

FIGURE 2.5. Effects of regularization on drag. *Left*: unregularized normal resistance coefficient r_n is indicated by dashed line, changes due to different δ-regularizations, $\delta \in \{10^{-4}, 5 \cdot 10^{-4}, 10^{-3}\}$, by solid lines. *Right*: δ-dependence of Stokes normal resistance $r_{n,S}$ and drag ratio $c_S = r_{\tau,S}/r_{n,S}$.

In the limit case of tangential flow, we particularly have the tangential force $\lim_{v_n \to 0} f_\tau(v_n, v_\tau) = v_\tau\, r_{\tau,S}$ and the derivative

$$\begin{aligned}\frac{\mathrm{d}\boldsymbol{f}}{\mathrm{d}\boldsymbol{v}}(\boldsymbol{\tau},\boldsymbol{v}) &= r_n^\delta(v_n)\,(\mathbf{I}-\boldsymbol{\tau}\otimes\boldsymbol{\tau}) + v_n (r_n^\delta)'(v_n)\,\boldsymbol{n}\otimes\boldsymbol{n} + r_\tau^\delta(v_n)\,\boldsymbol{\tau}\otimes\boldsymbol{\tau} + v_\tau (r_\tau^\delta)'(v_n)\,\boldsymbol{\tau}\otimes\boldsymbol{n} \\ &\overset{v_n\to 0}{\to} r_{n,S}\,(\mathbf{I}-\boldsymbol{\tau}\otimes\boldsymbol{\tau}) + r_{\tau,S}\,\boldsymbol{\tau}\otimes\boldsymbol{\tau}.\end{aligned}$$

with unit tensor $\mathbf{I}$, where the Stokes quantities $r_{n,S}$ and $r_{\tau,S}$ depend on the choice of δ, cf. (2.8) and Figure 2.5.

3. Splitting Approach

Coming back to the turbulent flow around a long flexible moving fiber, we generalize the drag by glueing together the locally valid results for the cylinder, imposing free-draining assumptions [29, 8]. Then, the drag force acting on the fiber at a certain position is given by

$$\boldsymbol{f}(\partial_s \boldsymbol{r}, \boldsymbol{u}(\boldsymbol{r},t) - \partial_t \boldsymbol{r}) = \boldsymbol{f}(\partial_s \boldsymbol{r}, (\bar{\boldsymbol{u}}(\boldsymbol{r},t) - \partial_t \boldsymbol{r}) + \boldsymbol{u}'(\boldsymbol{r},t)), \tag{3.1}$$

according to the RANS-averaging ansatz for the flow velocity, i.e., $\boldsymbol{u} = \bar{\boldsymbol{u}} + \boldsymbol{u}'$. As nonlinear functional on the centered Gaussian fluctuation velocity field $\boldsymbol{u}'$, the force is a stochastic process whose expectation and covariance can be computed according to the transformation theorem for random variables [4, 23]. However, due to the complexity, the efficient numerical handling of (3.1) is hopeless such that the Global-from-Local Force Concept [23] suggests its approximation by an appropriately chosen linear Gaussian drag force. Therefore, we split the drag force into a mean part $\boldsymbol{m}$ and a fluctuation part. The drag fluctuation inherits the stochastic properties of the turbulence by being modelled linearly in the velocity fluctuations with the matrix-valued linearization operator $\boldsymbol{L}$. We determine $\boldsymbol{m}$ and $\boldsymbol{L}$ as solution of the following optimization problem

$$\min_{\boldsymbol{m},\boldsymbol{L}} \frac{1}{(2\pi)^{3/2}} \int_{\mathbb{R}^3} \left(\boldsymbol{f}\left(\boldsymbol{\tau}, \boldsymbol{v} + \sqrt{\frac{2k}{3}}\boldsymbol{\xi}\right) - \boldsymbol{m}(\boldsymbol{\tau},\boldsymbol{v},k) - \boldsymbol{L}(\boldsymbol{\tau},\boldsymbol{v},k)\cdot\sqrt{\frac{2k}{3}}\boldsymbol{\xi} \right)^2 \exp\left(\frac{-\boldsymbol{\xi}^2}{2}\right) \mathrm{d}\boldsymbol{\xi}$$

where we incorporate the fact that the centered Gaussian velocity fluctuations are locally isotropic, i.e., the variance of every component satisfies $\mathbb{E}[(u_i')^2] = \mathbb{E}[\boldsymbol{u}'\cdot\boldsymbol{u}']/3 = 2k/3$ with turbulent kinetic energy k. So, the quantities $\boldsymbol{m}$ and $\boldsymbol{L}$ depend on the fiber orientation $\boldsymbol{\tau}$, the mean relative velocity $\boldsymbol{v}$ between mean flow and fiber and the turbulent kinetic energy k. By setting the variations of the cost functional with respect to the quantities equal to zero, we particularly obtain

$$\boldsymbol{m}(\boldsymbol{\tau},\boldsymbol{v},k) = \frac{1}{(2\pi)^{3/2}} \int_{\mathbb{R}^3} \boldsymbol{f}\left(\boldsymbol{\tau}, \boldsymbol{v} + \sqrt{\frac{2k}{3}}\boldsymbol{\xi}\right) \exp\left(\frac{-\boldsymbol{\xi}^2}{2}\right) \mathrm{d}\boldsymbol{\xi} \tag{3.2a}$$

$$\boldsymbol{L}(\boldsymbol{\tau},\boldsymbol{v},k) = \frac{1}{(2\pi)^{3/2}} \sqrt{\frac{3}{2k}} \int_{\mathbb{R}^3} \boldsymbol{f}\left(\boldsymbol{\tau}, \boldsymbol{v} + \sqrt{\frac{2k}{3}}\boldsymbol{\xi}\right) \otimes \boldsymbol{\xi} \exp\left(\frac{-\boldsymbol{\xi}^2}{2}\right) \mathrm{d}\boldsymbol{\xi}. \tag{3.2b}$$

For small turbulent kinetic energy, this linearization approach converges towards the Taylor expansion of first order presented in [24], i.e.,

$$\boldsymbol{m}(\boldsymbol{\tau},\boldsymbol{v},k) \to \boldsymbol{f}(\boldsymbol{\tau},\boldsymbol{v}), \qquad \boldsymbol{L}(\boldsymbol{\tau},\boldsymbol{v},k) \to \frac{\mathrm{d}\boldsymbol{f}}{\mathrm{d}\boldsymbol{v}}(\boldsymbol{\tau},\boldsymbol{v}) \qquad \text{for } k \to 0. \tag{3.3}$$

This simplification is a good approximation when the flow fluctuations are small perturbations to the mean relative velocity which is not true in general. In fact, $\sqrt{2k} = \|\boldsymbol{u}'\| \ll \|\bar{\boldsymbol{u}}\|$ according to the turbulence theory, but the relative velocity $\boldsymbol{v}(\boldsymbol{r},t) = \bar{\boldsymbol{u}}(\boldsymbol{r},t) - \partial_t \boldsymbol{r}$ between mean flow and fiber is only of the same order as the mean flow velocity $\bar{\boldsymbol{u}}$ in case of stiff, heavy fibers where $\partial_t \boldsymbol{r} \approx \boldsymbol{0}$. Flexible, light fibers, in contrast, move with the mean flow, i.e. $\boldsymbol{v} \approx \boldsymbol{0}$, such that $\sqrt{2k} \approx \|\boldsymbol{v}\|$ or even $\sqrt{2k} \gg \|\boldsymbol{v}\|$ might be expected. The general linearization approach (3.2) includes all these cases.

From the dimensionless quantities considered above we return to the associated dimensional ones that are used in the fiber dynamics model (1.1) by re-scaling with the typical mass $\rho \mathrm{d}^3$, the typical length d and the typical time d^2/ν (compare with the respective non-dimensionalization of the drag force $\mathbf{f}$, $\boldsymbol{f}$ in (2.1)). Hence, we obtain

$$\mathbf{m}(\boldsymbol{\tau},\mathbf{v},\mathrm{k},\nu,\rho,\mathrm{d}) = \frac{\rho\nu^2}{\mathrm{d}}\, \boldsymbol{m}\left(\boldsymbol{\tau}, \frac{\mathrm{d}}{\nu}\mathbf{v}, \frac{\mathrm{d}^2}{\nu^2}\mathrm{k}\right) \qquad \mathbf{L}(\boldsymbol{\tau},\mathbf{v},\mathrm{k},\nu,\rho,\mathrm{d}) = \rho\nu\, \boldsymbol{L}\left(\boldsymbol{\tau}, \frac{\mathrm{d}}{\nu}\mathbf{v}, \frac{\mathrm{d}^2}{\nu^2}\mathrm{k}\right).$$

For the numerical evaluation of the multiple integrals over the unbounded domain with Gaussian weight in expression (3.2), product Gauss-Hermite quadrature rules or Monte-Carlo methods can be applied traditionally, see e.g. [7, 9]. Moreover, recent works suggest efficient fully symmetric interpolatory rules [11] as well as stochastic algorithms with higher accuracy and better convergence properties than the simple Monte-Carlo methods for high-dimensional integrals [12].

4. Turbulence Correlation Model

The random part of the drag force acting on the fiber is crucially determined by the underlying turbulent velocity fluctuations that can asymptotically be approximated by Gaussian white noise with flow-dependent amplitude. The amplitude $\mathbf{D}$ represents hereby the integral effects of the localized centered Gaussian velocity fluctuations on the relevant fiber scales, containing the necessary information of the spatial and temporal double-velocity correlations. In an incompressible, homogeneous and isotropic turbulent flow, $\mathbf{D}$ particularly depends on the turbulence properties, i.e. turbulent kinetic energy k, dissipation rate ϵ and kinematic viscosity ν, as well as on the specific fiber-flow relation, i.e. mean relative velocity $\mathbf{v}$ and fiber orientation $\boldsymbol{\tau}$, $\|\boldsymbol{\tau}\|_2 = 1$. Non-dimensionalizing the correlation representant $\mathbf{D}$, the mean velocity $\mathbf{v}$ and the viscosity ν with the typical turbulent length $\mathrm{k}^{3/2}/\epsilon$ and time k/ϵ yields a reduction of the dependencies,

$$\mathbf{D}(\boldsymbol{\tau},\mathbf{v},\mathrm{k},\epsilon,\nu) = \frac{\mathrm{k}^{7/4}}{\epsilon}\, \boldsymbol{D}\left(\boldsymbol{\tau}, \frac{1}{\sqrt{\mathrm{k}}}\mathbf{v}, \frac{\epsilon}{\mathrm{k}^2}\nu\right), \qquad \mathbf{v} = \sqrt{\mathrm{k}}\boldsymbol{v}, \quad \nu = \frac{\mathrm{k}^2}{\epsilon}\zeta. \tag{4.1}$$

In the following we focus on the derivation of the dimensionless quantity $\boldsymbol{D}(\boldsymbol{\tau},\boldsymbol{v},\zeta)$. With the chosen non-dimensionalization, ζ is not only the dimensionless viscosity but also the ratio of turbulent fine-scale and large-scale length [40].

In an homogeneous turbulent flow, the tensor $\boldsymbol{\gamma} : (\mathbb{R}^3 \times \mathbb{R}_0^+)^2 \to \mathbb{R}^{3\times3}$ containing the spatial and temporal correlations of the double-velocity fluctuations,

$$\boldsymbol{\gamma}(\boldsymbol{x}+\hat{\boldsymbol{x}}, t+\hat{t}, \hat{\boldsymbol{x}}, \hat{t}) = \mathbb{E}[\boldsymbol{u'}(\boldsymbol{x}+\hat{\boldsymbol{x}}, t+\hat{t}) \otimes \boldsymbol{u'}(\hat{\boldsymbol{x}}, \hat{t})],$$

is invariant with regard to spatial and temporal translations. Hence it depends only on the differences of the arguments, $\boldsymbol{\gamma}(\boldsymbol{x}+\hat{\boldsymbol{x}}, t+\hat{t}, \hat{\boldsymbol{x}}, \hat{t}) = \boldsymbol{\gamma}(\boldsymbol{x}, t, \mathbf{0}, 0)$. The dynamic decay of the correlations might be modelled according to Taylor's hypothesis of frozen turbulence pattern [34] (originally proposed in [23] and incorporated in [24]), i.e. the fluctuations arise due to so-called turbulence pattern that are transported by the mean flow without changing their structure, $\boldsymbol{\gamma}(\boldsymbol{x}, t, \mathbf{0}, 0) = \boldsymbol{\gamma}_0(\boldsymbol{x} - t\bar{\boldsymbol{u}})$ with initial correlation tensor $\boldsymbol{\gamma}_0$. This hypothesis is based on the observation that the rate of decay of the mean properties is rather slow with respect to the time scale of the fluctuating fine-scale structures. However, considering the suspension of fibers in turbulent flows, the simulation results in [24] show that this ansatz might lead to unrealistic turbulent drag forces: short light fibers tending to move with the mean flow field would experience permanently the same non-varying fluctuations. Thus, we suggest to weaken the artificial frozen turbulence pattern by incorporating a natural temporal decay of the correlations (see [10] for details about the evolution of turbulence)

$$\boldsymbol{\gamma}(\boldsymbol{x}+\hat{\boldsymbol{x}}, t+\hat{t}, \hat{\boldsymbol{x}}, \hat{t}) = \boldsymbol{\gamma}_0(\boldsymbol{x} - t\bar{\boldsymbol{u}})\ \varphi(t). \tag{4.2}$$

The decay function φ satisfies $\varphi(0) = 1$ which implies that the integral of its Fourier transform $\mathcal{F}_\varphi$ is normalized. In particular, we use an exponential temporal decay, i.e.

$$\varphi(t) = \exp(-t^2/2), \qquad \mathcal{F}_\varphi(\omega) = \frac{1}{\sqrt{2\pi}}\exp(-\omega^2/2). \tag{4.3}$$

In the chosen non-dimensional formulation the typical decay time k/ϵ that acts as standard deviation in φ is scaled to one.* For the description of the initial correlation tensor $\boldsymbol{\gamma}_0$, it is also convenient to introduce its Fourier transform $\mathcal{F}_{\boldsymbol{\gamma}_0}$ that is known as spectral density in the turbulence theory. In case of incompressible isotropic turbulence the spectral density can be expressed exclusively in terms of the scalar-valued energy spectrum E

$$\mathcal{F}_{\boldsymbol{\gamma}_0}(\boldsymbol{\kappa}) = \frac{1}{(2\pi)^3}\int_{\mathbb{R}^3} \exp(-i\boldsymbol{\kappa}\cdot\boldsymbol{x})\,\boldsymbol{\gamma}_0(\boldsymbol{x})\,\mathrm{d}\boldsymbol{x} = \frac{1}{4\pi}\frac{E(\kappa)}{\kappa^2}\left(\mathbf{I} - \frac{1}{\kappa^2}\boldsymbol{\kappa}\otimes\boldsymbol{\kappa}\right)$$

with wave number $\kappa = \|\boldsymbol{\kappa}\|_2$. This relation holds analogously in the dimensional form, where the energy spectrum is scaled with the factor $\mathrm{k}^{5/2}/\epsilon$. The energy spectrum of isotropic turbulence was a well-studied topic of research during the last century (see references in [10, 14]). In particular, Kolmogorov's universal equilibrium theory was trend setting. Based on dimensional analysis he derived not only the characteristic ranges but also the typical run of the spectrum which agree with later coming physical concepts and experiments, cf. Kolmogorov's 5/3-Law and his hypothesis of local isotropy [10]. Gathering the existing knowledge about the energy spectrum, the following function that fulfills the requirements of the universal equilibrium theory and of the stochastic k-ϵ turbulence model was proposed in dimensional form in [23].

Energy Spectrum. *The twice continuously differentiable energy spectrum*

$$E(\kappa,\zeta) = C_{\mathrm{K}}\begin{cases} \kappa_1^{-5/3}\sum_{j=4}^{6} a_j\,(\frac{\kappa}{\kappa_1})^j & \kappa < \kappa_1 \\ \kappa^{-5/3} & \kappa_1 \le \kappa \le \kappa_2 \\ \kappa_2^{-5/3}\sum_{j=7}^{9} b_j\,(\frac{\kappa}{\kappa_2})^{-j} & \kappa_2 < \kappa \end{cases}, \tag{4.4a}$$

where the ζ-dependent transition wave numbers κ_1 and κ_2 are implicitly given by

$$\int_0^\infty E(\kappa,\zeta)\,\mathrm{d}\kappa = 1, \qquad \int_0^\infty E(\kappa,\zeta)\,\kappa^2\,\mathrm{d}\kappa = \frac{1}{2\zeta}, \tag{4.4b}$$

induces a differentiable velocity fluctuation field that stands in accordance to the k-ϵ *turbulence model. The regularity parameters are $a_4 = 230/9$, $a_5 = -391/9$, $a_6 = 170/9$, $b_7 = 209/9$, $b_8 = -352/9$, $b_9 = 152/9$, and the Kolmogorov constant is $C_{\mathrm{K}} = 1/2$.*

The integral conditions in (4.4b) can be reformulated as nonlinear system for κ_1 and κ_2 in ζ

$$\hat{a}_1\kappa_1^{-2/3} - \hat{b}_1\kappa_2^{-2/3} = C_K^{-1}, \qquad -\hat{a}_2\kappa_1^{4/3} + \hat{b}_2\kappa_2^{4/3} = (2C_K\zeta)^{-1},$$

with positive parameters

$$\hat{a}_1 = \frac{3}{2} + \sum_{j=4}^{6}\frac{a_j}{j+1}, \quad \hat{a}_2 = \frac{3}{4} - \sum_{j=4}^{6}\frac{a_j}{j+3}, \quad \hat{b}_1 = \frac{3}{2} - \sum_{j=7}^{9}\frac{b_j}{j-1}, \quad \hat{b}_2 = \frac{3}{4} + \sum_{j=7}^{9}\frac{b_j}{j-3}.$$

The condition $0 < \kappa_1 < \kappa_2 < \infty$ is equivalent to $0 < \zeta < \zeta_{crit} = (2C_K^3(\hat{b}_2 - \hat{a}_2)(\hat{b}_1 - \hat{a}_1)^2)^{-1} \approx 3.86$. The bounds on ζ (where we have $\kappa_1 = \kappa_2 = (C_K(\hat{a}_1 - \hat{b}_1))^{3/2}$ for $\zeta = \zeta_{crit}$ and $\kappa_1 = (C_K\hat{a}_1)^{3/2}$, $\kappa_2 = \infty$ for $\zeta = 0$) are no practically relevant restrictions, since the general turbulence theory assumes the ratio of fine-scale and large-scale length to satisfy $\zeta = \epsilon\nu/\mathrm{k}^2 \ll 1$.

The ζ-dependence that enters the model of the energy spectrum E via the consistency condition to the k-ϵ turbulence approach (4.4b) is handed over to the correlation tensor. Applying the correlation model (4.2), the turbulent drag amplitude $\boldsymbol{D}$ representing the integral effects of velocity

*For completeness we supplement the dimensional forms of the decay function $\phi(\mathrm{t}) = \exp(-\mathrm{t}^2/\mathrm{t}_{\mathrm{T}}^2)$ and its Fourier transform $\mathcal{F}_\phi(\varpi) = \mathrm{t}_{\mathrm{T}}\exp(-\mathrm{t}_{\mathrm{T}}^2\varpi^2/2)/\sqrt{2\pi}$ with $\mathrm{t}_{\mathrm{T}} = \mathrm{k}/\epsilon$. For slow decay $\mathrm{t}_{\mathrm{T}} \to \infty$ we obtain the desired transition to frozen turbulence $\phi(\mathrm{t}) \to 1$ and $\mathcal{F}_\phi(\varpi) \to \delta_0(\varpi)$ with Dirac distribution δ_0.

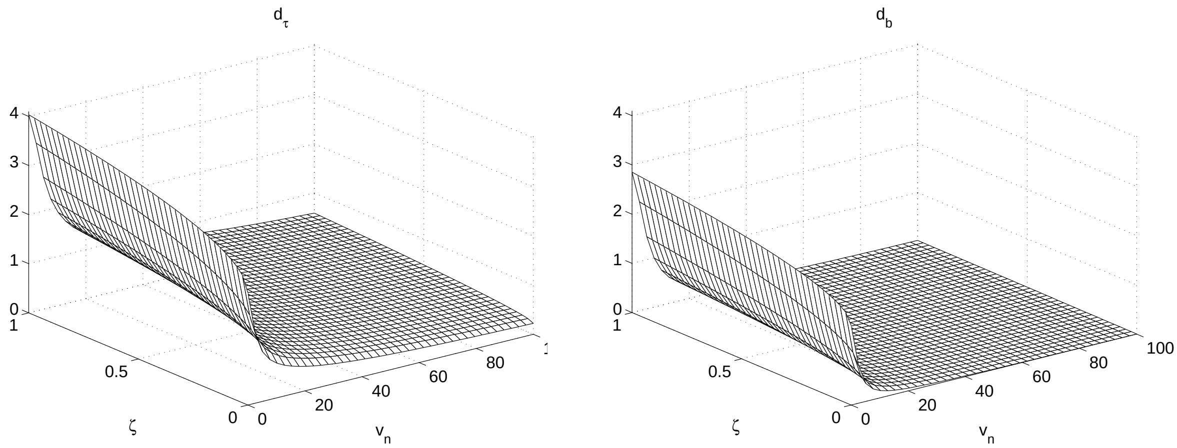

FIGURE 4.6. Tangential d_τ and binormal d_b amplitude.

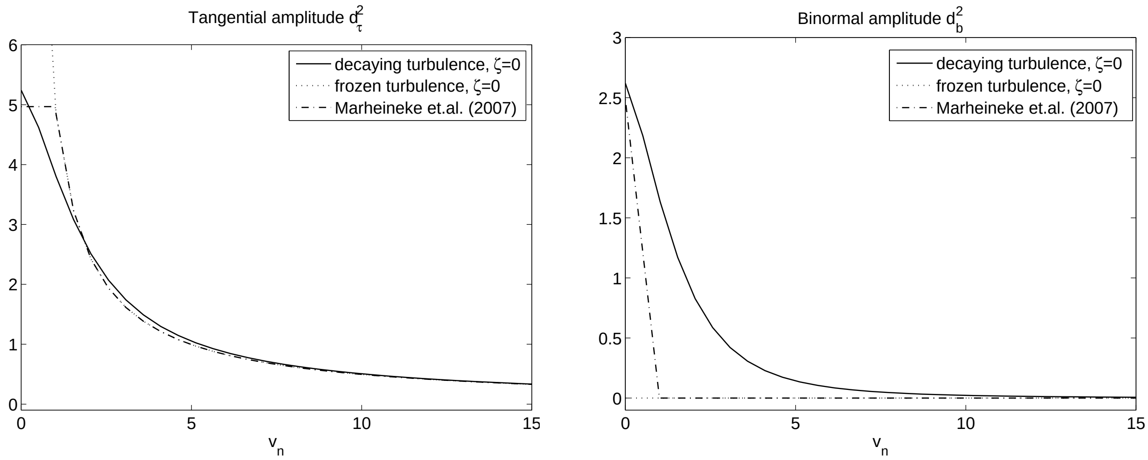

FIGURE 4.7. Convergence of $d_\tau^2(v_n, 0)$ and $d_b^2(v_n, 0)$, $v_n \to \infty$, to frozen turbulence results and amplitude proposed in [24].

fluctuations on the relevant fiber scales has the form

$$\begin{aligned}\boldsymbol{D}^2(\boldsymbol{\tau}, \boldsymbol{v}, \zeta) &= \int_{\mathbb{R}^2} \boldsymbol{\gamma}_0(s\boldsymbol{\tau} - t\boldsymbol{v}, \zeta)\ \varphi(t)\,\mathrm{d}s\,\mathrm{d}t\\ &= \pi \int_{\mathbb{R}^3} \frac{E(\kappa,\zeta)}{\kappa^2}(\mathbf{I} - \frac{1}{\kappa^2}\boldsymbol{\kappa}\otimes\boldsymbol{\kappa})\ \delta_0(\boldsymbol{\tau}\cdot\boldsymbol{\kappa})\ \mathcal{F}_\varphi(\boldsymbol{v}\cdot\boldsymbol{\kappa})\,\mathrm{d}\boldsymbol{\kappa},\end{aligned}$$

when inserting the Fourier transforms. In the $(\boldsymbol{\tau}, \boldsymbol{v})$-induced orthonormal basis $(\boldsymbol{n}, \boldsymbol{b}, \boldsymbol{\tau})$ where $\boldsymbol{v}\cdot\boldsymbol{b} = 0$, we obtain in particular

$$\boldsymbol{D}(\boldsymbol{\tau}, \boldsymbol{v}, \zeta) = d_n(v_n,\zeta)\,\boldsymbol{n}\otimes\boldsymbol{n} + d_b(v_n,\zeta)\,\boldsymbol{b}\otimes\boldsymbol{b} + d_\tau(v_n,\zeta)\,\boldsymbol{\tau}\otimes\boldsymbol{\tau}, \tag{4.5}$$

$$d^2_{n,b,\tau}(v_n,\zeta) = 4\pi\int_0^\infty \frac{E(\kappa,\zeta)}{\kappa}\, l_{n,b,\tau}(v_n\kappa)\,\mathrm{d}\kappa, \quad l_{n,b,\tau}(\kappa) = \int_0^{\pi/2} \{\sin^2\beta, \cos^2\beta, 1\}\,\mathcal{F}_\varphi(\kappa\cos\beta)\,\mathrm{d}\beta.$$

For this transformation we perform the integration over κ_τ and introduce polar coordinates $\kappa_n = \kappa\cos\beta$ and $\kappa_b = \kappa\sin\beta$. The angle integration over $[0, 2\pi]$ can be put down to the integration over the first quadrant because of the symmetry of the integrand. The coefficients d_i, $i = n, b, \tau$, in (4.5) obviously satisfy $d_n^2 + d_b^2 = d_\tau^2$ such that the effort for the computation of the tensor-valued amplitude $\boldsymbol{D}$ reduces to the evaluation of two scalar-valued functions d_τ, d_b depending on two parameters, Figure 4.6. Thereby, the influence of ζ is marginal and might be neglected in the numerical simulations in Section 5. Moreover, we obtain $\kappa l_\tau(\kappa) \to 1/2$ and $\kappa l_b(\kappa) \to 0$ in the limit $\kappa \to \infty$ which coincides with the results of frozen turbulence. The amplitude that we recently proposed in [24] corresponds to frozen turbulence with $\zeta = 0$ and a slight modification for $v_n < 1$. For a comparison to our representant of decaying turbulence (4.5) see Figure 4.7.

5. Application and Validation

In this section we show the applicability of our proposed stochastic force model to the simulation of practically relevant fiber-turbulence interactions. We validate the model with regard to experimental data coming from an industrial melt-spinning process of nonwoven materials.

5.1. **Numerical Treatment.** The system (1.1) of stochastic partial differential equation with algebraic constraint that models the fiber dynamics in turbulent flows is implemented in the software tool FIDYST†. Starting with the flow computation, e.g. via the commercial tool FLUENT, the relevant flow data (mean velocity $\bar{\mathbf{u}}$, kinetic energy k, dissipation rate ϵ etc.) enter into the routine for the fiber dynamics where the nonlinear stochastic fiber system is solved by a method of lines. Thereby, the use of a spatial finite difference method of higher order ensures the appropriate approximation of the algebraic constraint. The Box-Muller method generates the Gaussian deviates for the stochastic force. Incorporating the force amplitude on the interpolated flow data explicitly, a semi-implicit Euler method realizes the time integration. An adaptive time step control gives stability and accuracy. The resulting nonlinear system of equations is finally solved by a Newton method.

5.2. **Set-up of Measurements and Simulations.** Fiber-turbulence interactions are of great importance in melt-spinning processes of nonwoven materials. Here, thousands of individual fibers are obtained by continuous extrusion of a molten polymer granular that is spun through narrow jets and stretched by cooling air flows to crystallize. The resulting flexible slender fibers are then entangled by a highly turbulent air flow and laid down onto a conveyor belt to form a web. The properties of this web and hence the quality of the nonwoven material depend essentially on the dynamics of the fibers in the turbulent deposition region. In the following, we focus exclusively on this region taking the crystallization for granted and considering the fibers as elastic. The turbulence causes entanglement and loop forming along the fibers, which yields slower vertical fiber velocities, wider deposition ranges and higher isotropic properties of the nonwoven material. To validate our stochastic model, we could compare either the statistical fiber velocities in the deposition region or the statistical material properties of the resulting products, e.g. mass distribution, fiber orientation.

†FIDYST: Fiber Dynamics Simulation Tool developed at Fraunhofer ITWM, Kaiserslautern

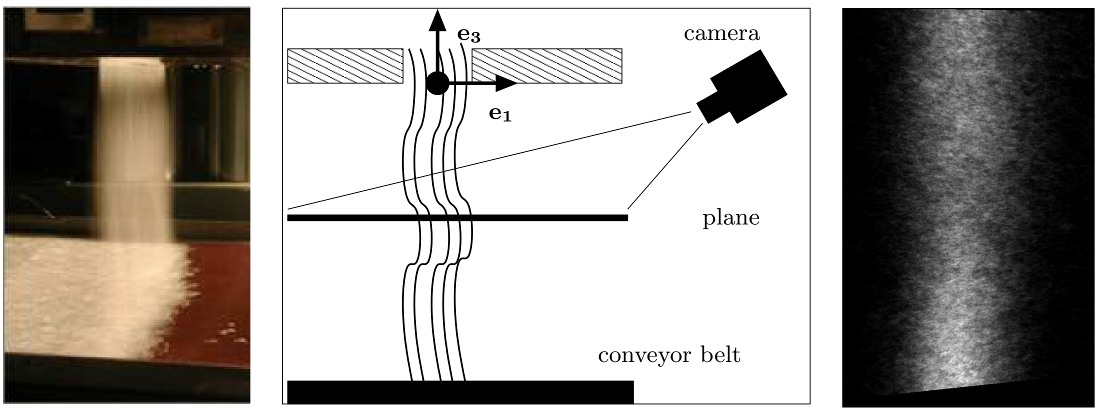

Figure 5.8. *From left to right:* deposition of fiber curtain in a laminar flow, PIV set-up, recorded fiber structures in light sheet (photos by industrial partners).

The last is easy to measure, but has the decisive disadvantage that the nonwoven material shows not only the effects of the turbulence but also of the lay-down, e.g. buckling behavior, friction, conveyor belt speed. Admittedly, this is also valid for the fiber dynamics near the conveyor belt. Hence, to exclude this perturbing influence, we consider the fibers that enter the region. However, measuring their velocities turns out to be a technically delicate task.

The particle image velocimetry (PIV) is a planar laser light sheet technique [28] in that a light sheet is pulsed twice and the images of the structures lying in this plane are recorded on a photograph, see Figure 5.8. The technique enables the determination of their planar displacements and thus of their planar velocities. Dividing the image plane into small interrogation spots and cross correlating the sequential frames from two time exposures, the spatial change of the image structures are computed by means of a peak detection, i.e. the displacement that generates the maximal cross correlation approximates statistically the average displacement in the cell. With regard to the time between the laser pulses, this yields then the velocity associated with each spot. Perturbed or defective data are thereby filtered by prescribed tolerances. As for our endless fibers cutting a light sheet parallel to the conveyor belt, PIV follows the trajectories of the fibers in the plane and measures their planar velocities. These differ from the instantaneous velocities. Consider the PIV set-up as sketched in Figure 5.8 with fixed outer orthonormal basis $(\mathbf{e_1}, \mathbf{e_2}, \mathbf{e_3})$. Then, the fiber velocity in a plane h is given by the total time derivative of $\mathbf{r}(\mathrm{s}_{track}(\mathrm{t}), \mathrm{t}) = \eta_1(\mathrm{t})\mathbf{e_1} + \eta_2(\mathrm{t})\mathbf{e_2} + \mathrm{h}\mathbf{e_3}$. The vanishing of the vertical planar velocity implies the temporal change $\partial_\mathrm{t} \mathrm{s}_{track} = -\partial_\mathrm{t} \mathrm{r}_3 / \partial_\mathrm{s} \mathrm{r}_3$ of the implicitly defined function s_{track}. Inserting this relation in the expression for the horizontal components yields

$$\mathrm{w}_i(t) := \partial_\mathrm{t} \eta_i(t) = \left(\partial_\mathrm{t} \mathrm{r}_i - \partial_\mathrm{t} \mathrm{r}_3 \frac{\partial_\mathrm{s} \mathrm{r}_i}{\partial_\mathrm{s} \mathrm{r}_3} \right) (\mathrm{s}_{track}(\mathrm{t}), \mathrm{t}), \;\; i = 1, 2, \qquad \mathrm{r}_3(\mathrm{s}_{track}(\mathrm{t}), \mathrm{t}) = \mathrm{h}, \tag{5.1}$$

with $\mathrm{r}_i = \mathbf{r} \cdot \mathbf{e_i}$, $i = 1, 2, 3$. The dominance of the second summand in the first equation of (5.1) depends on the orientation of the fiber with respect to the plane. In case of parallelism which might occur due to loop forming, we obtain even infinite planar fiber velocities in spite of finite instantaneous quantities. But they are filtered by a tolerance threshold.

The experiments and PIV-measurements are performed and provided by our industrial partner. The experiments are set up for hundreds of slender endless fibers that are suspended in a highly turbulent flow with periodically oscillating mean stream in $\mathbf{e_1}$-direction. The streamlines are exemplarily visualized in Figure 5.9. The periodic motion causes a respective delayed oscillation and a widening of the fiber curtain. This is taken into account in measurements and simulations to obtain comparable data. The PIV-measurements provide information about the fiber density and the velocity distribution in two planes, i.e. near the entry (plane E) and in the middle of the deposition region (plane M), at eight equidistant time points within in the periodic sequence. To obtain a large, statistically equivalent random sample, we simulate the dynamics of the fiber curtain by means of

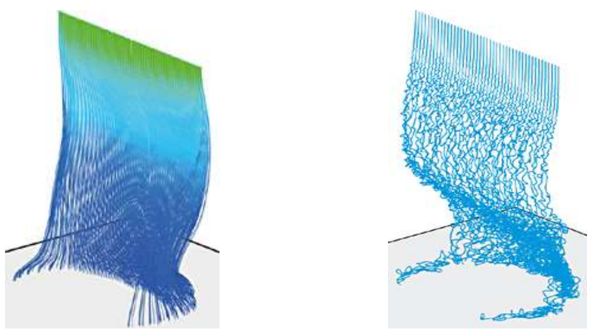

FIGURE 5.9. Industrial set-up for measurements and simulations. *Left:* streamlines of periodically oscillating mean flow field simulated with FLUENT. *Right:* corresponding fiber curtain, fiber motion is computed with FIDYST using $\delta = 10^{-5}$, (3.3) and $\zeta = 0$ in (4.1).

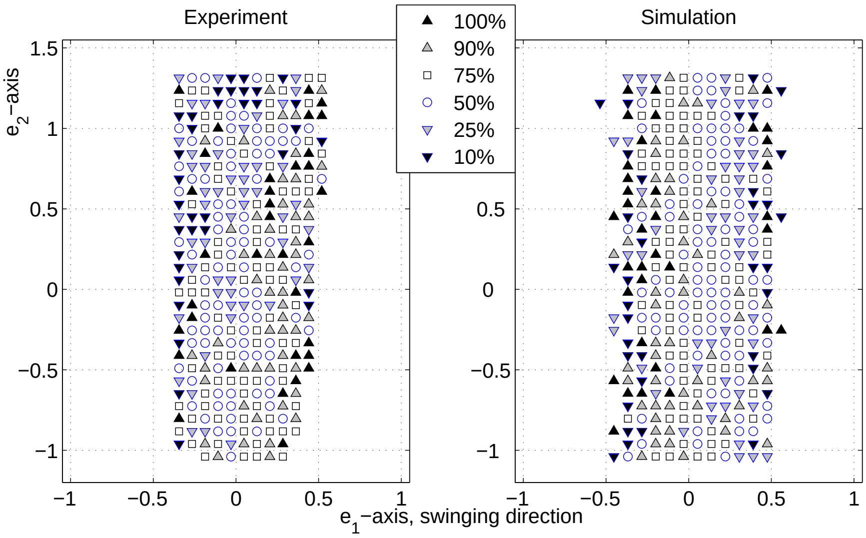

FIGURE 5.10. Hitting spots of fiber curtain in plane M at certain time point, colored by quantiles of velocity component w_1. (Quantile 10% includes all points where the associated w_1 belongs to the lowest 10% of all w_1-values, quantile 25% includes all points where w_1 lies between the lowest 10-25% etc.)

66 individual fibers for a respective number of oscillations. As for the stochastic drag model, we use the simplifications $\zeta = 0$ in the computation (4.1) of the turbulence amplitude $\mathbf{D}$ as well as (3.3) in the splitting approach for $\mathbf{m}$, $\mathbf{L}$. The last approximation avoids the numerical evaluation of the multiple integrals in (3.2) and speeds up the computations drastically. The slenderness ratio of the fibers is $\delta = 10^{-5}$. Their endless character and their deposition onto the conveyor belt are realized by appropriate boundary conditions and constraints with contact forces to (1.1). Possible fiber-fiber interactions are neglected such that the calculations can be additionally accelerated by parallelizing the independent fiber motions. Then, they take around 30 h CPU-time on a cluster with 66 Intel Xeon processors, 2.4 GHz.

5.3. **Results.** The measured and simulated results for the planar fiber velocities and the fiber curtain dynamics are presented statistically. Thereby, the length and velocity values in the following diagrams are scaled with problem-specific length and velocity scales such that they can be understood as relative quantities. The periodic time sequence is considered as $[0, 1]$.

According to the PIV-measurements, the planes M and E are divided into small quadratic cells to that the average velocity components w_1, w_2, the variances $\mathrm{Var}(w_1)$, $\mathrm{Var}(w_2)$ and the covariance $\mathrm{Cov}(w_1, w_2)$ are associated. These are computed from the sample of all photographs / simulations corresponding to a specific temporal scene. Figure 5.10 exemplarily illustrates the hitting spots in plane M for a certain time point and gives thus the instantaneous position and width of the fiber curtain, cf. photo of light sheet in Figure 5.8. The spots are thereby colored in terms of the velocity w_1 in swinging direction $\mathbf{e_1}$. To emphasize the extreme velocities, we use the representation of quantiles: the dark up- and down-directed triangles mark the high velocities in positive and negative $\mathbf{e_1}$-direction, respectively. They occur in general at the boundary. Since their appearance is hardly correlated to the swinging direction, the geometrical second term in (5.1) dominates the planar velocity. Therefore, we might conclude much loop forming of the single fibers which agrees with Figure 5.9.

Both, experimental and numerical results, satisfy Gaussian distributions for all planar velocity variations whose discrete probability distribution functions are exemplified for a single scene in Figure 5.11. Focusing on their characteristic parameters, i.e. expectation μ and standard deviation σ, the expectations coincide very well. This is also true for their dynamics in plane M and E, see

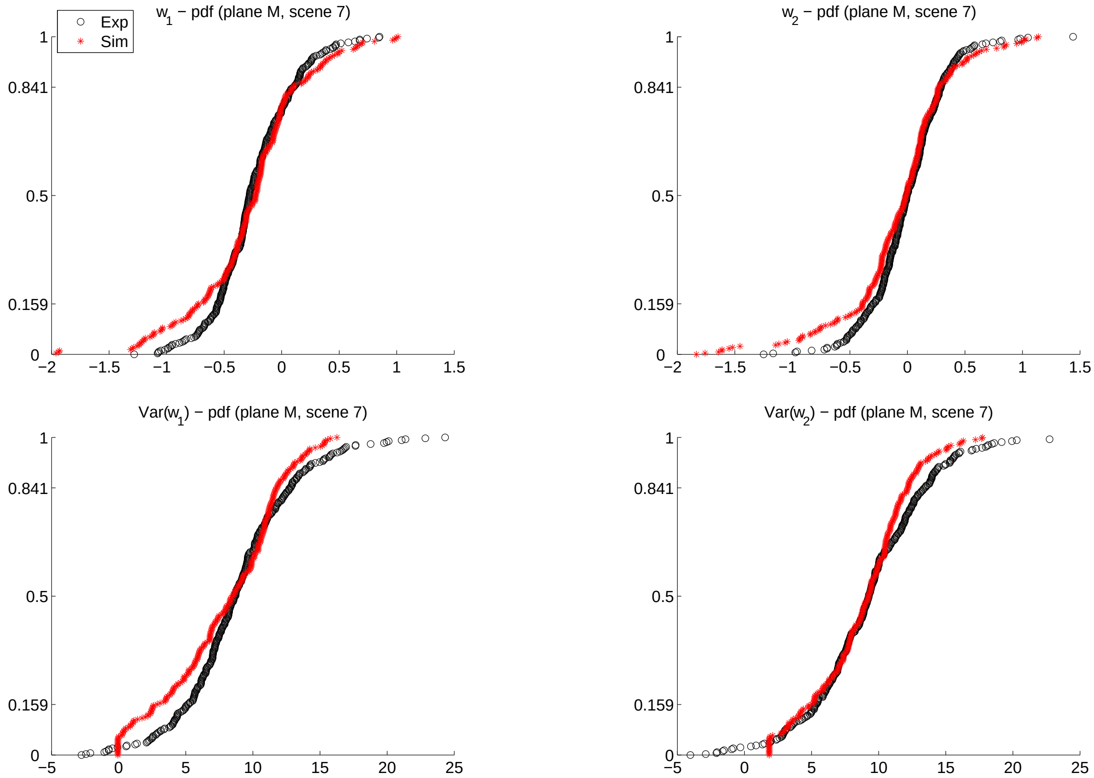

FIGURE 5.11. Discrete probability distribution functions $\mathcal{F}$ for w_1, w_2, Var(w_1), Var(w_2) in plane M at specific scene. Experimental results are marked by black ($\circ$) and simulated by red ($\star$). (Expectation μ and standard deviation σ can be estimated from the plot, $\mu \approx \mathcal{F}^{-1}(0.5)$, $\sigma \approx \mathcal{F}^{-1}(0.841) - \mu \approx \mu - \mathcal{F}^{-1}(0.159)$.)

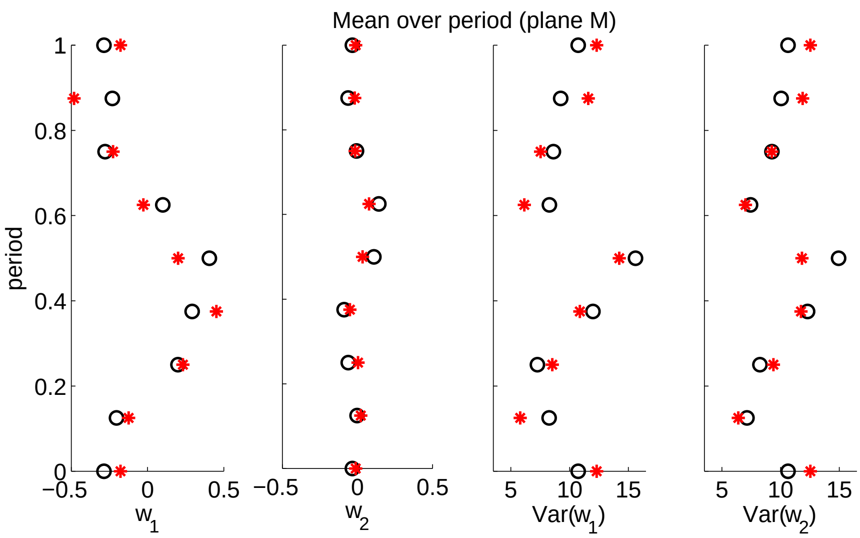

FIGURE 5.12. Dynamics of expectation μ for velocity variations in plane M over time period. Experimental results are marked by black ($\circ$), simulated by red ($\star$).

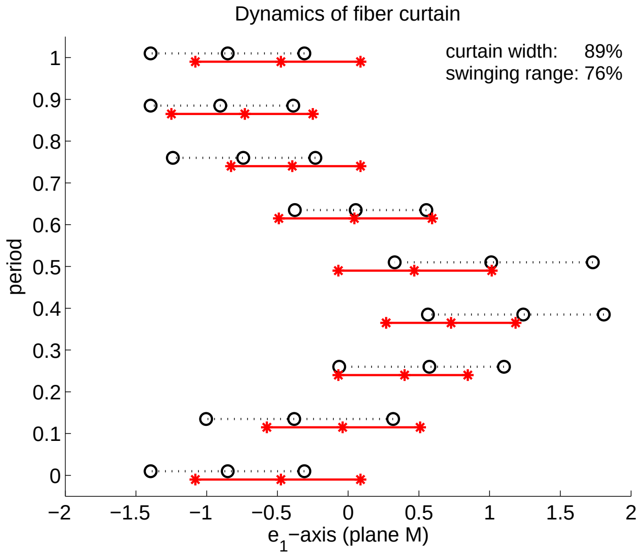

FIGURE 5.13. Dynamics of fiber curtain in plane M. Experimental results for curtain center, boundaries and width are represented by black marker (∘) and dotted line (:), simulated results by red marker (⋆) and solid line (−).

Figure 5.12 for plane M. The standard deviations in contrast show differences. We observe the tendency that the experimental data describe very uniform standard deviations over the time period. This rises the suspect of fiber bunch forming (fiber clusters on light sheet) in combination with the application of a good filtering algorithm. Since neither the experimental tolerances nor accuracies are known, the adaptation of the simulations is difficult. The observed differences might be simply caused by the use of various thresholds.

The dynamics of the simulated fiber curtain agrees qualitatively well with the experimental results, see Figure 5.13 for plane M. The fiber curtain is small around the symmetry axis and becomes wider in the turning points. But, exactly here, the simulated curtain is quantitatively too small which leads to a underestimation of the average curtain width and thus of the resulting swinging range. This underestimate might come from the neglect of fiber-fiber interactions and sticky fiber bunches. As the drag coefficients are proportional to the fiber diameter, thicker ropes experience larger uniform forces that obviously cause a higher impulse and hence stronger oscillations. This remains to be investigated. However, note that the simplifying assumptions reduce the computational effort and allow indeed the simulation of curtains consisting of many fibers.

We conclude this section with the visualization of a spinning process of nonwoven materials that shows fiber dynamics, deposition and fleece forming (Figure 5.14). To emphasize the effects of our stochastic force model, we simulate non-interacting slender fibers in a turbulent flow field with stationary, vertically directed mean stream.

6. CONCLUSION

In this paper we have developed an improved stochastic aerodynamic force model based on the concepts of [23] that allows the simulation of long slender elastic fibers immersed in turbulent flows. The underlying drag model is uniformly valid for all Reynolds number regimes and incident flow directions. It is composed of asymptotic Oseen and Stokes theory, Taylor heuristic and numerical simulations and is overall concordant with the experimental studies in literature. The practical relevance of our stochastic drag force has been shown for the application of technical textile manufacturing. In particular, we have validated the simulation results with PIV-measurements of hundreds of fibers in a melt-spinning process of nonwoven materials. Although the reliability of

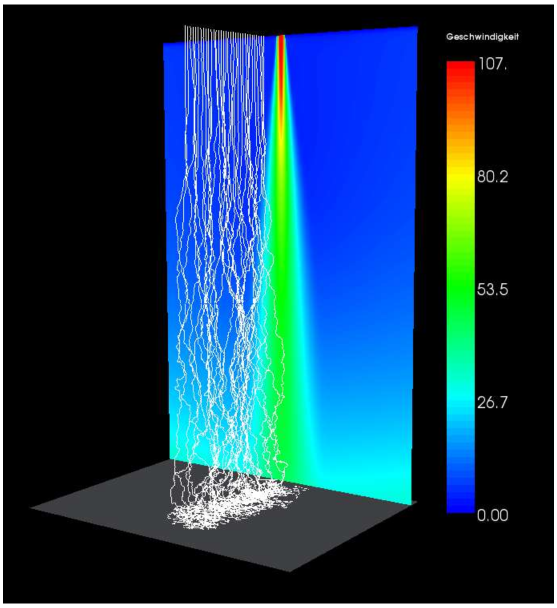

FIGURE 5.14. Simulation of spinning process: fibers immersed in a turbulent flow. The color bar prescribes the velocity magnitude of the stationary, vertically directed mean flow field.

the PIV-measurements as reference data concerning the planar fiber velocities might be questioned as long as the used filter tolerances are not specified in detail, the received agreements of simulated and measured probability distributions, mean velocity values and fiber curtain characteristics are very promising and militate in favor of our stochastic force model.

When the dynamics of dense sticky fiber bunches / curtains in turbulent flows is of interest, the affection of the turbulence by the flexible structure plays a crucial role and has certainly to be taken into account in a two-way coupling for the fiber-fluid interactions. In this context, the fiber bunches might be treated as a continuous porous medium whose properties could be deduced from a statistical analysis of a large set of individual fibers via an homogenization approach. This remains to be investigated.

ACKNOWLEDGEMENTS. Our special thanks go to our colleague Ferdinand Olawsky, Fraunhofer ITWM, for the FIDYST simulations and to our industrial partner for the PIV-measurements. This work has been supported by Rheinland-Pfalz Excellence Center for Mathematical and Computational Modeling $(CM)^2$ and by Deutsche Forschungsgemeinschaft (DFG), WE 2003/3-1.

REFERENCES

[1] S. S. ANTMAN, *Nonlinear Problems of Elasticity*, Springer Verlag, New York, 2004.
[2] L. BAIRSTOW, B. M. CAVE, AND E. D. LANG, *The resistance of a cylinder moving in a viscous fluid*, Proceedings of the Royal Society London, A, 100 (1923), pp. 394–413.
[3] G. K. BATCHELOR, *Slender-body theory for particles of arbitrary cross-section in Stokes flow*, Journal of Fluid Mechanics, 44 (1970), pp. 419–440.
[4] E. BEHRENDS, *Mass- und Integrationstheorie*, Springer Verlag, Berlin, 1987.
[5] E. CHADWICK AND N. FISHWICK, *Lift on slender boldies with elliptical cross section evaluated by using an Oseen flow model*, SIAM Journal of Applied Mathematics, 67 (2007), pp. 1465–1478.
[6] R. G. COX, *The motion of long slender bodies in a viscous fluid. Part 1. General theory*, Journal of Fluid Mechanics, 44 (1970), pp. 791–810.
[7] P. J. DAVIS AND P. RABINOWITZ, *Methods of Numerical Integration*, Acadamic Press, New York, 1984.
[8] M. DOI AND D. CHEN, *Simulation of aggregating coilloids in shear flow*, Journal of Chemical Physics, 90 (1989), pp. 5271–5279.
[9] M. EVANS AND T. SWARTZ, *Some integration strategies for problems in statistical interference*, Computing Science and Statistics, 24 (1992), pp. 310–317.

[10] U. Frisch, *Turbulence. The Legacy of A. N. Kolmogorov*, Cambridge University Press, 1995.

[11] A. Genz and B. Keister, *Fully symmetric interpolatory rules for multiple integrals over infinite regions with Gaussian weight*, Journal of Computational and Applied Mathematics, 71 (1996), pp. 299–309.

[12] A. Genz and J. Monahan, *A stochastic algorithm for high dimensional multiple integrals over unbounded regions with Gaussian weight*, Journal of Computational and Applied Mathematics, 112 (1999), pp. 71–81.

[13] T. Götz and A. Unterreiter, *Analysis and numerics of an integral equation model for slender bodies in low-Reynolds-number flow*, Journal of Integral Equations and Applications, 12 (2000), pp. 225–270.

[14] O. Hinze, *Turbulence*, McGraw-Hill, New York, 2 ed., 1975.

[15] S. F. Hoerner, *Fluid-dynamic drag. Practical information on aerodynamic drag and hydrodynamic resistance.* Published by the author. Obtainable from ISVA., 1965.

[16] I. Imai, *On the asymptotic behaviour of viscous fluid flow at a great distance from a cylindrical body, with special reference to Filon's paradox*, Proceedings of the Royal Society London, A, 208 (1951), pp. 487–516.

[17] ———, *Theory of bluff bodies.* Technical Note BN-220, University of Maryland, Institute Fluid Mechanics, 1957.

[18] S. Kaplun, *Low Reynolds number flow past a circular cylinder*, Journal Mathematical Mechanics, 6 (1937), pp. 595–603.

[19] J. B. Keller and S. I. Rubinow, *Slender-body theory for slow viscous flow*, Journal of Fluid Mechanics, 75 (1976), pp. 705–714.

[20] H. Lamb, *On the uniform motion of a sphere through a viscous fluid*, Philosophical Magazine, 6 (1911), pp. 113–121.

[21] B. E. Launder and B. I. Sharma, *Application of the energy dissipation model of turbulence to the calculation of flow near a spinning disc*, Letters in Heat and Mass Transfer, 1 (1974), pp. 131–138.

[22] D. Lucor and G. E. Karniadakis, *Effects of oblique inflow in vortex-induced vibrations*, Flow, Turbulence and Compustion, 71 (2003), pp. 375–389.

[23] N. Marheineke and R. Wegener, *Fiber dynamics in turbulent flows: General modeling framework*, SIAM Journal of Applied Mathematics, 66 (2006), pp. 1703–1726.

[24] ———, *Fiber dynamics in turbulent flows: Specific Taylor drag*, SIAM Journal of Applied Mathematics, 68 (2007), pp. 1–23.

[25] J. A. Olsen and R. J. Kerekes, *The motion of fibres in turbulent flow*, Journal of Fluid Mechanics, 337 (1998), pp. 47–64.

[26] L. M. Pismen and A. Nir, *On the motion of suspended particles in stationary homogeneous turbulence*, Journal of Fluid Mechanics, 84 (1978), pp. 193–206.

[27] I. Proudman and J. R. A. Pearson, *Expansions at small Reynolds numbers for the flow past a sphere and a circular cylinder*, Journal of Fluid Mechanics, 1 (1957), pp. 237–262.

[28] M. Raffel, C. Willert, and J. Kompenhans, *Particle Image Velocimetry, A Practical Guide*, Springer Verlag, Berlin, 1998.

[29] F. R. Russel and D. J. Klingenberg, *Dynamic simulation of flexible fibers composed of linked rigid bodies*, Journal of Chemical Physics, 105 (1997), pp. 2949–2960.

[30] G. Schewe, *On the force fluctuations acting on a circular cylinder in cross-flow from subcritical up to transcritical Reynolds numbers*, Journal of Fluid Mechanics, 133 (1983), pp. 265–285.

[31] H. Schlichting, *Grenzschicht-Theorie*, Verlag G. Braun, Karlsruhe, 1982.

[32] T. H. Shih and J. L. Lumley, *Second-order modelling of particle dispersion in a turbulent flow*, Journal of Fluid Mechanics, 163 (1986), pp. 349–363.

[33] B. M. Sumer and J. Fredsoe, *Hydrodynamics around cylindrical structures*, World Scientific Publishing, 2006.

[34] G. I. Taylor, *The spectrum of turbulence*, Proceedings of the Royal Society London, A, 164 (1938), pp. 476–490.

[35] ———, *Analysis of the swimming of long and narrow animals*, Proceedings of the Royal Society London, A, 214 (1952), pp. 158–183.

[36] S. Tomotika and T. Aoi, *An expansion formula for the drag on a circular cylinder moivng through a viscous fluid at small Reynolds number*, Quarterly Journal Mechanics Applied Mathematics, 4 (1951), pp. 401–406.

[37] S. Tomotika, T. Aoi, and H. Yosinobu, *On the forces acting on a circular cylinder set obliquely in a uniform stream at low values of Reynolds number*, Proceedings of the Royal Society London, A, 219 (1953), pp. 233–244.

[38] D. J. Tritton, *Experiments on the flow past circular cylinder at low Reynolds number*, Journal of Fluid Mechanics, 6 (1959), pp. 547–567.

[39] B. Underwood, *Random-walk modeling of turbulent impaction to a smooth wall*, International Journal of Multiphase Flow, 19 (1993), pp. 485–500.

[40] D. C. Wilcox, *Turbulence Modeling for CFD*, DCW Industries, 2 ed., 1998.

[41] M. M. Zdravkovich, *Flow around circular cylinders, Vol 1: Fundamentals*, Oxford University Press, New York, 1997.

N. Marheineke, Johannes-Gutenberg Universität, Institut für Mathematik, D-55099 Mainz, Germany
E-mail address: `marheineke@mathematik.uni-kl.de`

R. Wegener, Fraunhofer ITWM, D-67663 Kaiserslautern, Germany
E-mail address: `wegener@mathematik.uni-kl.de`

Published reports of the Fraunhofer ITWM

The PDF-files of the following reports are available under:
www.itwm.fraunhofer.de/de/zentral__berichte/berichte

1. D. Hietel, K. Steiner, J. Struckmeier
A Finite - Volume Particle Method for Compressible Flows
(19 pages, 1998)

2. M. Feldmann, S. Seibold
Damage Diagnosis of Rotors: Application of Hilbert Transform and Multi-Hypothesis Testing
Keywords: Hilbert transform, damage diagnosis, Kalman filtering, non-linear dynamics
(23 pages, 1998)

3. Y. Ben-Haim, S. Seibold
Robust Reliability of Diagnostic Multi-Hypothesis Algorithms: Application to Rotating Machinery
Keywords: Robust reliability, convex models, Kalman filtering, multi-hypothesis diagnosis, rotating machinery, crack diagnosis
(24 pages, 1998)

4. F.-Th. Lentes, N. Siedow
Three-dimensional Radiative Heat Transfer in Glass Cooling Processes
(23 pages, 1998)

5. A. Klar, R. Wegener
A hierarchy of models for multilane vehicular traffic
Part I: Modeling
(23 pages, 1998)

Part II: Numerical and stochastic investigations
(17 pages, 1998)

6. A. Klar, N. Siedow
Boundary Layers and Domain Decomposition for Radiative Heat Transfer and Diffusion Equations: Applications to Glass Manufacturing Processes
(24 pages, 1998)

7. I. Choquet
Heterogeneous catalysis modelling and numerical simulation in rarified gas flows
Part I: Coverage locally at equilibrium
(24 pages, 1998)

8. J. Ohser, B. Steinbach, C. Lang
Efficient Texture Analysis of Binary Images
(17 pages, 1998)

9. J. Orlik
Homogenization for viscoelasticity of the integral type with aging and shrinkage
(20 pages, 1998)

10. J. Mohring
Helmholtz Resonators with Large Aperture
(21 pages, 1998)

11. H. W. Hamacher, A. Schöbel
On Center Cycles in Grid Graphs
(15 pages, 1998)

12. H. W. Hamacher, K.-H. Küfer
Inverse radiation therapy planning - a multiple objective optimisation approach
(14 pages, 1999)

13. C. Lang, J. Ohser, R. Hilfer
On the Analysis of Spatial Binary Images
(20 pages, 1999)

14. M. Junk
On the Construction of Discrete Equilibrium Distributions for Kinetic Schemes
(24 pages, 1999)

15. M. Junk, S. V. Raghurame Rao
A new discrete velocity method for Navier-Stokes equations
(20 pages, 1999)

16. H. Neunzert
Mathematics as a Key to Key Technologies
(39 pages (4 PDF-Files), 1999)

17. J. Ohser, K. Sandau
Considerations about the Estimation of the Size Distribution in Wicksell's Corpuscle Problem
(18 pages, 1999)

18. E. Carrizosa, H. W. Hamacher, R. Klein, S. Nickel
Solving nonconvex planar location problems by finite dominating sets
Keywords: Continuous Location, Polyhedral Gauges, Finite Dominating Sets, Approximation, Sandwich Algorithm, Greedy Algorithm
(19 pages, 2000)

19. A. Becker
A Review on Image Distortion Measures
Keywords: Distortion measure, human visual system
(26 pages, 2000)

20. H. W. Hamacher, M. Labbé, S. Nickel, T. Sonneborn
Polyhedral Properties of the Uncapacitated Multiple Allocation Hub Location Problem
Keywords: integer programming, hub location, facility location, valid inequalities, facets, branch and cut
(21 pages, 2000)

21. H. W. Hamacher, A. Schöbel
Design of Zone Tariff Systems in Public Transportation
(30 pages, 2001)

22. D. Hietel, M. Junk, R. Keck, D. Teleaga
The Finite-Volume-Particle Method for Conservation Laws
(16 pages, 2001)

23. T. Bender, H. Hennes, J. Kalcsics, M. T. Melo, S. Nickel
Location Software and Interface with GIS and Supply Chain Management
Keywords: facility location, software development, geographical information systems, supply chain management
(48 pages, 2001)

24. H. W. Hamacher, S. A. Tjandra
Mathematical Modelling of Evacuation Problems: A State of Art
(44 pages, 2001)

25. J. Kuhnert, S. Tiwari
Grid free method for solving the Poisson equation
Keywords: Poisson equation, Least squares method, Grid free method
(19 pages, 2001)

26. T. Götz, H. Rave, D. Reinel-Bitzer, K. Steiner, H. Tiemeier
Simulation of the fiber spinning process
Keywords: Melt spinning, fiber model, Lattice Boltzmann, CFD
(19 pages, 2001)

27. A. Zemitis
On interaction of a liquid film with an obstacle
Keywords: impinging jets, liquid film, models, numerical solution, shape
(22 pages, 2001)

28. I. Ginzburg, K. Steiner
Free surface lattice-Boltzmann method to model the filling of expanding cavities by Bingham Fluids
Keywords: Generalized LBE, free-surface phenomena, interface boundary conditions, filling processes, Bingham viscoplastic model, regularized models
(22 pages, 2001)

29. H. Neunzert
»Denn nichts ist für den Menschen als Menschen etwas wert, was er nicht mit Leidenschaft tun kann«
Vortrag anlässlich der Verleihung des Akademiepreises des Landes Rheinland-Pfalz am 21.11.2001
Keywords: Lehre, Forschung, angewandte Mathematik, Mehrskalenanalyse, Strömungsmechanik
(18 pages, 2001)

30. J. Kuhnert, S. Tiwari
Finite pointset method based on the projection method for simulations of the incompressible Navier-Stokes equations
Keywords: Incompressible Navier-Stokes equations, Meshfree method, Projection method, Particle scheme, Least squares approximation
AMS subject classification: 76D05, 76M28
(25 pages, 2001)

31. R. Korn, M. Krekel
Optimal Portfolios with Fixed Consumption or Income Streams
Keywords: Portfolio optimisation, stochastic control, HJB equation, discretisation of control problems
(23 pages, 2002)

32. M. Krekel
Optimal portfolios with a loan dependent credit spread
Keywords: Portfolio optimisation, stochastic control, HJB equation, credit spread, log utility, power utility, non-linear wealth dynamics
(25 pages, 2002)

33. J. Ohser, W. Nagel, K. Schladitz
The Euler number of discretized sets – on the choice of adjacency in homogeneous lattices
Keywords: image analysis, Euler number, neighborhod relationships, cuboidal lattice
(32 pages, 2002)

34. I. Ginzburg, K. Steiner
Lattice Boltzmann Model for Free-Surface flow and Its Application to Filling Process in Casting
Keywords: Lattice Boltzmann models; free-surface phenomena; interface boundary conditions; filling processes; injection molding; volume of fluid method; interface boundary conditions; advection-schemes; upwind-schemes
(54 pages, 2002)

35. M. Günther, A. Klar, T. Materne, R. Wegener
Multivalued fundamental diagrams and stop and go waves for continuum traffic equations
Keywords: traffic flow, macroscopic equations, kinetic derivation, multivalued fundamental diagram, stop and go waves, phase transitions
(25 pages, 2002)

36. S. Feldmann, P. Lang, D. Prätzel-Wolters
Parameter influence on the zeros of network determinants
Keywords: Networks, Equicofactor matrix polynomials, Realization theory, Matrix perturbation theory
(30 pages, 2002)

37. K. Koch, J. Ohser, K. Schladitz
Spectral theory for random closed sets and estimating the covariance via frequency space
Keywords: Random set, Bartlett spectrum, fast Fourier transform, power spectrum
(28 pages, 2002)

38. D. d'Humières, I. Ginzburg
Multi-reflection boundary conditions for lattice Boltzmann models
Keywords: lattice Boltzmann equation, boudary condistions, bounce-back rule, Navier-Stokes equation
(72 pages, 2002)

39. R. Korn
Elementare Finanzmathematik
Keywords: Finanzmathematik, Aktien, Optionen, Portfolio-Optimierung, Börse, Lehrerweiterbildung, Mathematikunterricht
(98 pages, 2002)

40. J. Kallrath, M. C. Müller, S. Nickel
Batch Presorting Problems: Models and Complexity Results
Keywords: Complexity theory, Integer programming, Assigment, Logistics
(19 pages, 2002)

41. J. Linn
On the frame-invariant description of the phase space of the Folgar-Tucker equation
Key words: fiber orientation, Folgar-Tucker equation, injection molding
(5 pages, 2003)

42. T. Hanne, S. Nickel
A Multi-Objective Evolutionary Algorithm for Scheduling and Inspection Planning in Software Development Projects
Key words: multiple objective programming, project management and scheduling, software development, evolutionary algorithms, efficient set
(29 pages, 2003)

43. T. Bortfeld , K.-H. Küfer, M. Monz, A. Scherrer, C. Thieke, H. Trinkaus
Intensity-Modulated Radiotherapy - A Large Scale Multi-Criteria Programming Problem
Keywords: multiple criteria optimization, representative systems of Pareto solutions, adaptive triangulation, clustering and disaggregation techniques, visualization of Pareto solutions, medical physics, external beam radiotherapy planning, intensity modulated radiotherapy
(31 pages, 2003)

44. T. Halfmann, T. Wichmann
Overview of Symbolic Methods in Industrial Analog Circuit Design
Keywords: CAD, automated analog circuit design, symbolic analysis, computer algebra, behavioral modeling, system simulation, circuit sizing, macro modeling, differential-algebraic equations, index
(17 pages, 2003)

45. S. E. Mikhailov, J. Orlik
Asymptotic Homogenisation in Strength and Fatigue Durability Analysis of Composites
Keywords: multiscale structures, asymptotic homogenization, strength, fatigue, singularity, non-local conditions
(14 pages, 2003)

46. P. Domínguez-Marín, P. Hansen, N. Mladenovi ́c , S. Nickel
Heuristic Procedures for Solving the Discrete Ordered Median Problem
Keywords: genetic algorithms, variable neighborhood search, discrete facility location
(31 pages, 2003)

47. N. Boland, P. Domínguez-Marín, S. Nickel, J. Puerto
Exact Procedures for Solving the Discrete Ordered Median Problem
Keywords: discrete location, Integer programming
(41 pages, 2003)

48. S. Feldmann, P. Lang
Padé-like reduction of stable discrete linear systems preserving their stability
Keywords: Discrete linear systems, model reduction, stability, Hankel matrix, Stein equation
(16 pages, 2003)

49. J. Kallrath, S. Nickel
A Polynomial Case of the Batch Presorting Problem
Keywords: batch presorting problem, online optimization, competetive analysis, polynomial algorithms, logistics
(17 pages, 2003)

50. T. Hanne, H. L. Trinkaus
knowCube for MCDM – Visual and Interactive Support for Multicriteria Decision Making
Key words: Multicriteria decision making, knowledge management, decision support systems, visual interfaces, interactive navigation, real-life applications.
(26 pages, 2003)

51. O. Iliev, V. Laptev
On Numerical Simulation of Flow Through Oil Filters
Keywords: oil filters, coupled flow in plain and porous media, Navier-Stokes, Brinkman, numerical simulation
(8 pages, 2003)

52. W. Dörfler, O. Iliev, D. Stoyanov, D. Vassileva
On a Multigrid Adaptive Refinement Solver for Saturated Non-Newtonian Flow in Porous Media
Keywords: Nonlinear multigrid, adaptive refinement, non-Newtonian flow in porous media
(17 pages, 2003)

53. S. Kruse
On the Pricing of Forward Starting Options under Stochastic Volatility
Keywords: Option pricing, forward starting options, Heston model, stochastic volatility, cliquet options
(11 pages, 2003)

54. O. Iliev, D. Stoyanov
Multigrid – adaptive local refinement solver for incompressible flows
Keywords: Navier-Stokes equations, incompressible flow, projection-type splitting, SIMPLE, multigrid methods, adaptive local refinement, lid-driven flow in a cavity
(37 pages, 2003)

55. V. Starikovicius
The multiphase flow and heat transfer in porous media
Keywords: Two-phase flow in porous media, various formulations, global pressure, multiphase mixture model, numerical simulation
(30 pages, 2003)

56. P. Lang, A. Sarishvili, A. Wirsen
Blocked neural networks for knowledge extraction in the software development process
Keywords: Blocked Neural Networks, Nonlinear Regression, Knowledge Extraction, Code Inspection
(21 pages, 2003)

57. H. Knaf, P. Lang, S. Zeiser
Diagnosis aiding in Regulation Thermography using Fuzzy Logic
Keywords: fuzzy logic,knowledge representation, expert system
(22 pages, 2003)

58. M. T. Melo, S. Nickel, F. Saldanha da Gama
Largescale models for dynamic multicommodity capacitated facility location
Keywords: supply chain management, strategic planning, dynamic location, modeling
(40 pages, 2003)

59. J. Orlik
Homogenization for contact problems with periodically rough surfaces
Keywords: asymptotic homogenization, contact problems
(28 pages, 2004)

60. A. Scherrer, K.-H. Küfer, M. Monz, F. Alonso, T. Bortfeld
IMRT planning on adaptive volume structures – a significant advance of computational complexity
Keywords: Intensity-modulated radiation therapy (IMRT), inverse treatment planning, adaptive volume structures, hierarchical clustering, local refinement, adaptive clustering, convex programming, mesh generation, multi-grid methods
(24 pages, 2004)

61. D. Kehrwald
Parallel lattice Boltzmann simulation of complex flows
Keywords: Lattice Boltzmann methods, parallel computing, microstructure simulation, virtual material design, pseudo-plastic fluids, liquid composite moulding
(12 pages, 2004)

62. O. Iliev, J. Linn, M. Moog, D. Niedziela, V. Starikovicius
On the Performance of Certain Iterative Solvers for Coupled Systems Arising in Discretization of Non-Newtonian Flow Equations

Keywords: Performance of iterative solvers, Preconditioners, Non-Newtonian flow
(17 pages, 2004)

63. R. Ciegis, O. Iliev, S. Rief, K. Steiner
On Modelling and Simulation of Different Regimes for Liquid Polymer Moulding
Keywords: Liquid Polymer Moulding, Modelling, Simulation, Infiltration, Front Propagation, non-Newtonian flow in porous media
(43 pages, 2004)

64. T. Hanne, H. Neu
Simulating Human Resources in Software Development Processes
Keywords: Human resource modeling, software process, productivity, human factors, learning curve
(14 pages, 2004)

65. O. Iliev, A. Mikelic, P. Popov
Fluid structure interaction problems in deformable porous media: Toward permeability of deformable porous media
Keywords: fluid-structure interaction, deformable porous media, upscaling, linear elasticity, stokes, finite elements
(28 pages, 2004)

66. F. Gaspar, O. Iliev, F. Lisbona, A. Naumovich, P. Vabishchevich
On numerical solution of 1-D poroelasticity equations in a multilayered domain
Keywords: poroelasticity, multilayered material, finite volume discretization, MAC type grid
(41 pages, 2004)

67. J. Ohser, K. Schladitz, K. Koch, M. Nöthe
Diffraction by image processing and its application in materials science
Keywords: porous microstructure, image analysis, random set, fast Fourier transform, power spectrum, Bartlett spectrum
(13 pages, 2004)

68. H. Neunzert
Mathematics as a Technology: Challenges for the next 10 Years
Keywords: applied mathematics, technology, modelling, simulation, visualization, optimization, glass processing, spinning processes, fiber-fluid interaction, trubulence effects, topological optimization, multicriteria optimization, Uncertainty and Risk, financial mathematics, Malliavin calculus, Monte-Carlo methods, virtual material design, filtration, bio-informatics, system biology
(29 pages, 2004)

69. R. Ewing, O. Iliev, R. Lazarov, A. Naumovich
On convergence of certain finite difference discretizations for 1D poroelasticity interface problems
Keywords: poroelasticity, multilayered material, finite volume discretizations, MAC type grid, error estimates
(26 pages,2004)

70. W. Dörfler, O. Iliev, D. Stoyanov, D. Vassileva
On Efficient Simulation of Non-Newtonian Flow in Saturated Porous Media with a Multigrid Adaptive Refinement Solver
Keywords: Nonlinear multigrid, adaptive renement, non-Newtonian in porous media
(25 pages, 2004)

71. J. Kalcsics, S. Nickel, M. Schröder
Towards a Unified Territory Design Approach – Applications, Algorithms and GIS Integration
Keywords: territory desgin, political districting, sales territory alignment, optimization algorithms, Geographical Information Systems
(40 pages, 2005)

72. K. Schladitz, S. Peters, D. Reinel-Bitzer, A. Wiegmann, J. Ohser
Design of acoustic trim based on geometric modeling and flow simulation for non-woven
Keywords: random system of fibers, Poisson line process, flow resistivity, acoustic absorption, Lattice-Boltzmann method, non-woven
(21 pages, 2005)

73. V. Rutka, A. Wiegmann
Explicit Jump Immersed Interface Method for virtual material design of the effective elastic moduli of composite materials
Keywords: virtual material design, explicit jump immersed interface method, effective elastic moduli, composite materials
(22 pages, 2005)

74. T. Hanne
Eine Übersicht zum Scheduling von Baustellen
Keywords: Projektplanung, Scheduling, Bauplanung, Bauindustrie
(32 pages, 2005)

75. J. Linn
The Folgar-Tucker Model as a Differetial Algebraic System for Fiber Orientation Calculation
Keywords: fiber orientation, Folgar–Tucker model, invariants, algebraic constraints, phase space, trace stability
(15 pages, 2005)

76. M. Speckert, K. Dreßler, H. Mauch, A. Lion, G. J. Wierda
Simulation eines neuartigen Prüfsystems für Achserprobungen durch MKS-Modellierung einschließlich Regelung
Keywords: virtual test rig, suspension testing, multibody simulation, modeling hexapod test rig, optimization of test rig configuration
(20 pages, 2005)

77. K.-H. Küfer, M. Monz, A. Scherrer, P. Süss, F. Alonso, A. S. A. Sultan, Th. Bortfeld, D. Craft, Chr. Thieke
Multicriteria optimization in intensity modulated radiotherapy planning
Keywords: multicriteria optimization, extreme solutions, real-time decision making, adaptive approximation schemes, clustering methods, IMRT planning, reverse engineering
(51 pages, 2005)

78. S. Amstutz, H. Andrä
A new algorithm for topology optimization using a level-set method
Keywords: shape optimization, topology optimization, topological sensitivity, level-set
(22 pages, 2005)

79. N. Ettrich
Generation of surface elevation models for urban drainage simulation
Keywords: Flooding, simulation, urban elevation models, laser scanning
(22 pages, 2005)

80. H. Andrä, J. Linn, I. Matei, I. Shklyar, K. Steiner, E. Teichmann
OPTCAST – Entwicklung adäquater Strukturoptimierungsverfahren für Gießereien Technischer Bericht (KURZFASSUNG)
Keywords: Topologieoptimierung, Level-Set-Methode, Gießprozesssimulation, Gießtechnische Restriktionen, CAE-Kette zur Strukturoptimierung
(77 pages, 2005)

81. N. Marheineke, R. Wegener
Fiber Dynamics in Turbulent Flows Part I: General Modeling Framework
Keywords: fiber-fluid interaction; Cosserat rod; turbulence modeling; Kolmogorov's energy spectrum; double-velocity correlations; differentiable Gaussian fields
(20 pages, 2005)

Part II: Specific Taylor Drag
Keywords: flexible fibers; k-ε turbulence model; fiber-turbulence interaction scales; air drag; random Gaussian aerodynamic force; white noise; stochastic differential equations; ARMA process
(18 pages, 2005)

82. C. H. Lampert, O. Wirjadi
An Optimal Non-Orthogonal Separation of the Anisotropic Gaussian Convolution Filter
Keywords: Anisotropic Gaussian filter, linear filtering, orientation space, nD image processing, separable filters
(25 pages, 2005)

83. H. Andrä, D. Stoyanov
Error indicators in the parallel finite element solver for linear elasticity DDFEM
Keywords: linear elasticity, finite element method, hierarchical shape functions, domain decom-position, parallel implementation, a posteriori error estimates
(21 pages, 2006)

84. M. Schröder, I. Solchenbach
Optimization of Transfer Quality in Regional Public Transit
Keywords: public transit, transfer quality, quadratic assignment problem
(16 pages, 2006)

85. A. Naumovich, F. J. Gaspar
On a multigrid solver for the three-dimensional Biot poroelasticity system in multilayered domains
Keywords: poroelasticity, interface problem, multigrid, operator-dependent prolongation
(11 pages, 2006)

86. S. Panda, R. Wegener, N. Marheineke
Slender Body Theory for the Dynamics of Curved Viscous Fibers
Keywords: curved viscous fibers; fluid dynamics; Navier-Stokes equations; free boundary value problem; asymptotic expansions; slender body theory
(14 pages, 2006)

87. E. Ivanov, H. Andrä, A. Kudryavtsev
Domain Decomposition Approach for Automatic Parallel Generation of Tetrahedral Grids
Key words: Grid Generation, Unstructured Grid, Delaunay Triangulation, Parallel Programming, Domain Decomposition, Load Balancing
(18 pages, 2006)

88. S. Tiwari, S. Antonov, D. Hietel, J. Kuhnert, R. Wegener
A Meshfree Method for Simulations of Interactions between Fluids and Flexible Structures
Key words: Meshfree Method, FPM, Fluid Structure Interaction, Sheet of Paper, Dynamical Coupling
(16 pages, 2006)

89. R. Ciegis , O. Iliev, V. Starikovicius, K. Steiner
Numerical Algorithms for Solving Problems of Multiphase Flows in Porous Media
Keywords: nonlinear algorithms, finite-volume method, software tools, porous media, flows
(16 pages, 2006)

90. D. Niedziela, O. Iliev, A. Latz
On 3D Numerical Simulations of Viscoelastic Fluids
Keywords: non-Newtonian fluids, anisotropic viscosity, integral constitutive equation
(18 pages, 2006)

91. A. Winterfeld
Application of general semi-infinite Programming to Lapidary Cutting Problems
Keywords: large scale optimization, nonlinear programming, general semi-infinite optimization, design centering, clustering
(26 pages, 2006)

92. J. Orlik, A. Ostrovska
Space-Time Finite Element Approximation and Numerical Solution of Hereditary Linear Viscoelasticity Problems
Keywords: hereditary viscoelasticity; kern approximation by interpolation; space-time finite element approximation, stability and a priori estimate
(24 pages, 2006)

93. V. Rutka, A. Wiegmann, H. Andrä
EJIIM for Calculation of effective Elastic Moduli in 3D Linear Elasticity
Keywords: Elliptic PDE, linear elasticity, irregular domain, finite differences, fast solvers, effective elastic moduli
(24 pages, 2006)

94. A. Wiegmann, A. Zemitis
EJ-HEAT: A Fast Explicit Jump Harmonic Averaging Solver for the Effective Heat Conductivity of Composite Materials
Keywords: Stationary heat equation, effective thermal conductivity, explicit jump, discontinuous coefficients, virtual material design, microstructure simulation, EJ-HEAT
(21 pages, 2006)

95. A. Naumovich
On a finite volume discretization of the three-dimensional Biot poroelasticity system in multilayered domains
Keywords: Biot poroelasticity system, interface problems, finite volume discretization, finite difference method
(21 pages, 2006)

96. M. Krekel, J. Wenzel
A unified approach to Credit Default Swaption and Constant Maturity Credit Default Swap valuation
Keywords: LIBOR market model, credit risk, Credit Default Swaption, Constant Maturity Credit Default Swap-method
(43 pages, 2006)

97. A. Dreyer
Interval Methods for Analog Circiuts
Keywords: interval arithmetic, analog circuits, tolerance analysis, parametric linear systems, frequency response, symbolic analysis, CAD, computer algebra
(36 pages, 2006)

98. N. Weigel, S. Weihe, G. Bitsch, K. Dreßler
Usage of Simulation for Design and Optimization of Testing
Keywords: Vehicle test rigs, MBS, control, hydraulics, testing philosophy
(14 pages, 2006)

99. H. Lang, G. Bitsch, K. Dreßler, M. Speckert
Comparison of the solutions of the elastic and elastoplastic boundary value problems
Keywords: Elastic BVP, elastoplastic BVP, variational inequalities, rate-independency, hysteresis, linear kinematic hardening, stop- and play-operator
(21 pages, 2006)

100. M. Speckert, K. Dreßler, H. Mauch
MBS Simulation of a hexapod based suspension test rig
Keywords: Test rig, MBS simulation, suspension, hydraulics, controlling, design optimization
(12 pages, 2006)

101. S. Azizi Sultan, K.-H. Küfer
A dynamic algorithm for beam orientations in multicriteria IMRT planning
Keywords: radiotherapy planning, beam orientation optimization, dynamic approach, evolutionary algorithm, global optimization
(14 pages, 2006)

102. T. Götz, A. Klar, N. Marheineke, R. Wegener
A Stochastic Model for the Fiber Lay-down Process in the Nonwoven Production
Keywords: fiber dynamics, stochastic Hamiltonian system, stochastic averaging
(17 pages, 2006)

103. Ph. Süss, K.-H. Küfer
Balancing control and simplicity: a variable aggregation method in intensity modulated radiation therapy planning
Keywords: IMRT planning, variable aggregation, clustering methods
(22 pages, 2006)

104. A. Beaudry, G. Laporte, T. Melo, S. Nickel
Dynamic transportation of patients in hospitals
Keywords: in-house hospital transportation, dial-a-ride, dynamic mode, tabu search
(37 pages, 2006)

105. Th. Hanne
Applying multiobjective evolutionary algorithms in industrial projects
Keywords: multiobjective evolutionary algorithms, discrete optimization, continuous optimization, electronic circuit design, semi-infinite programming, scheduling
(18 pages, 2006)

106. J. Franke, S. Halim
Wild bootstrap tests for comparing signals and images
Keywords: wild bootstrap test, texture classification, textile quality control, defect detection, kernel estimate, nonparametric regression
(13 pages, 2007)

107. Z. Drezner, S. Nickel
Solving the ordered one-median problem in the plane
Keywords: planar location, global optimization, ordered median, big triangle small triangle method, bounds, numerical experiments
(21 pages, 2007)

108. Th. Götz, A. Klar, A. Unterreiter, R. Wegener
Numerical evidance for the non-existing of solutions of the equations desribing rotational fiber spinning
Keywords: rotational fiber spinning, viscous fibers, boundary value problem, existence of solutions
(11 pages, 2007)

109. Ph. Süss, K.-H. Küfer
Smooth intensity maps and the Bortfeld-Boyer sequencer
Keywords: probabilistic analysis, intensity modulated radiotherapy treatment (IMRT), IMRT plan application, step-and-shoot sequencing
(8 pages, 2007)

110. E. Ivanov, O. Gluchshenko, H. Andrä, A. Kudryavtsev
Parallel software tool for decomposing and meshing of 3d structures
Keywords: a-priori domain decomposition, unstructured grid, Delaunay mesh generation
(14 pages, 2007)

111. O. Iliev, R. Lazarov, J. Willems
Numerical study of two-grid preconditioners for 1d elliptic problems with highly oscillating discontinuous coefficients
Keywords: two-grid algorithm, oscillating coefficients, preconditioner
(20 pages, 2007)

112. L. Bonilla, T. Götz, A. Klar, N. Marheineke, R. Wegener
Hydrodynamic limit of the Fokker-Planck-equation describing fiber lay-down processes
Keywords: stochastic dierential equations, Fokker-Planck equation, asymptotic expansion, Ornstein-Uhlenbeck process
(17 pages, 2007)

113. S. Rief
Modeling and simulation of the pressing section of a paper machine
Keywords: paper machine, computational fluid dynamics, porous media
(41 pages, 2007)

114. R. Ciegis, O. Iliev, Z. Lakdawala
On parallel numerical algorithms for simulating industrial filtration problems
Keywords: Navier-Stokes-Brinkmann equations, finite volume discretization method, SIMPLE, parallel computing, data decomposition method
(24 pages, 2007)

115. N. Marheineke, R. Wegener
Dynamics of curved viscous fibers with surface tension
Keywords: Slender body theory, curved viscous bers with surface tension, free boundary value problem
(25 pages, 2007)

116. S. Feth, J. Franke, M. Speckert
Resampling-Methoden zur mse-Korrektur und Anwendungen in der Betriebsfestigkeit
Keywords: Weibull, Bootstrap, Maximum-Likelihood, Betriebsfestigkeit
(16 pages, 2007)

117. H. Knaf
Kernel Fisher discriminant functions – a concise and rigorous introduction
Keywords: wild bootstrap test, texture classification, textile quality control, defect detection, kernel estimate, nonparametric regression
(30 pages, 2007)

118. O. Iliev, I. Rybak
On numerical upscaling for flows in heterogeneous porous media

Keywords: numerical upscaling, heterogeneous porous media, single phase flow, Darcy's law, multiscale problem, effective permeability, multipoint flux approximation, anisotropy
(17 pages, 2007)

119. O. Iliev, I. Rybak
On approximation property of multipoint flux approximation method
Keywords: Multipoint flux approximation, finite volume method, elliptic equation, discontinuous tensor coefficients, anisotropy
(15 pages, 2007)

120. O. Iliev, I. Rybak, J. Willems
On upscaling heat conductivity for a class of industrial problems
Keywords: Multiscale problems, effective heat conductivity, numerical upscaling, domain decomposition
(21 pages, 2007)

121. R. Ewing, O. Iliev, R. Lazarov, I. Rybak
On two-level preconditioners for flow in porous media
Keywords: Multiscale problem, Darcy's law, single phase flow, anisotropic heterogeneous porous media, numerical upscaling, multigrid, domain decomposition, efficient preconditioner
(18 pages, 2007)

122. M. Brickenstein, A. Dreyer
POLYBORI: A Gröbner basis framework for Boolean polynomials
Keywords: Gröbner basis, formal verification, Boolean polynomials, algebraic cryptoanalysis, satisfiability
(23 pages, 2007)

123. O. Wirjadi
Survey of 3d image segmentation methods
Keywords: image processing, 3d, image segmentation, binarization
(20 pages, 2007)

124. S. Zeytun, A. Gupta
A Comparative Study of the Vasicek and the CIR Model of the Short Rate
Keywords: interest rates, Vasicek model, CIR-model, calibration, parameter estimation
(17 pages, 2007)

125. G. Hanselmann, A. Sarishvili
Heterogeneous redundancy in software quality prediction using a hybrid Bayesian approach
Keywords: reliability prediction, fault prediction, non-homogeneous poisson process, Bayesian model averaging
(17 pages, 2007)

126. V. Maag, M. Berger, A. Winterfeld, K.-H. Küfer
A novel non-linear approach to minimal area rectangular packing
Keywords: rectangular packing, non-overlapping constraints, non-linear optimization, regularization, relaxation
(18 pages, 2007)

127. M. Monz, K.-H. Küfer, T. Bortfeld, C. Thieke
Pareto navigation – systematic multi-criteria-based IMRT treatment plan determination
Keywords: convex, interactive multi-objective optimization, intensity modulated radiotherapy planning
(15 pages, 2007)

128. M. Krause, A. Scherrer
On the role of modeling parameters in IMRT plan optimization
Keywords: intensity-modulated radiotherapy (IMRT), inverse IMRT planning, convex optimization, sensitivity analysis, elasticity, modeling parameters, equivalent uniform dose (EUD)
(18 pages, 2007)

129. A. Wiegmann
Computation of the permeability of porous materials from their microstructure by FFF-Stokes
Keywords: permeability, numerical homogenization, fast Stokes solver
(24 pages, 2007)

130. T. Melo, S. Nickel, F. Saldanha da Gama
Facility Location and Supply Chain Management – A comprehensive review
Keywords: facility location, supply chain management, network design
(54 pages, 2007)

131. T. Hanne, T. Melo, S. Nickel
Bringing robustness to patient flow management through optimized patient transports in hospitals
Keywords: Dial-a-Ride problem, online problem, case study, tabu search, hospital logistics
(23 pages, 2007)

132. R. Ewing, O. Iliev, R. Lazarov, I. Rybak, J. Willems
An efficient approach for upscaling properties of composite materials with high contrast of coefficients
Keywords: effective heat conductivity, permeability of fractured porous media, numerical upscaling, fibrous insulation materials, metal foams
(16 pages, 2008)

133. S. Gelareh, S. Nickel
New approaches to hub location problems in public transport planning
Keywords: integer programming, hub location, transportation, decomposition, heuristic
(25 pages, 2008)

134. G. Thömmes, J. Becker, M. Junk, A. K. Vaikuntam, D. Kehrwald, A. Klar, K. Steiner, A. Wiegmann
A Lattice Boltzmann Method for immiscible multiphase flow simulations using the Level Set Method
Keywords: Lattice Boltzmann method, Level Set method, free surface, multiphase flow
(28 pages, 2008)

135. J. Orlik
Homogenization in elasto-plasticity
Keywords: multiscale structures, asymptotic homogenization, nonlinear energy
(40 pages, 2008)

136. J. Almquist, H. Schmidt, P. Lang, J. Deitmer, M. Jirstrand, D. Prätzel-Wolters, H. Becker
Determination of interaction between MCT1 and CAII via a mathematical and physiological approach
Keywords: mathematical modeling; model reduction; electrophysiology; pH-sensitive microelectrodes; proton antenna
(20 pages, 2008)

137. E. Savenkov, H. Andrä, O. Iliev
An analysis of one regularization approach for solution of pure Neumann problem
Keywords: pure Neumann problem, elasticity, regularization, finite element method, condition number
(27 pages, 2008)

138. O. Berman, J. Kalcsics, D. Krass, S. Nickel
The ordered gradual covering location problem on a network
Keywords: gradual covering, ordered median function, network location
(32 pages, 2008)

139. S. Gelareh, S. Nickel
Multi-period public transport design: A novel model and solution approaches
Keywords: Integer programming, hub location, public transport, multi-period planning, heuristics
(31 pages, 2008)

140. T. Melo, S. Nickel, F. Saldanha-da-Gama
Network design decisions in supply chain planning
Keywords: supply chain design, integer programming models, location models, heuristics
(20 pages, 2008)

141. C. Lautensack, A. Särkkä, J. Freitag, K. Schladitz
Anisotropy analysis of pressed point processes
Keywords: estimation of compression, isotropy test, nearest neighbour distance, orientation analysis, polar ice, Ripley's K function
(35 pages, 2008)

142. O. Iliev, R. Lazarov, J. Willems
A Graph-Laplacian approach for calculating the effective thermal conductivity of complicated fiber geometries
Keywords: graph laplacian, effective heat conductivity, numerical upscaling, fibrous materials
(14 pages, 2008)

143. J. Linn, T. Stephan, J. Carlsson, R. Bohlin
Fast simulation of quasistatic rod deformations for VR applications
Keywords: quasistatic deformations, geometrically exact rod models, variational formulation, energy minimization, finite differences, nonlinear conjugate gradients
(7 pages, 2008)

144. J. Linn, T. Stephan
Simulation of quasistatic deformations using discrete rod models
Keywords: quasistatic deformations, geometrically exact rod models, variational formulation, energy minimization, finite differences, nonlinear conjugate gradients
(9 pages, 2008)

145. J. Marburger, N. Marheineke, R. Pinnau
Adjoint based optimal control using meshless discretizations
Keywords: Mesh-less methods, particle methods, Eulerian-Lagrangian formulation, optimization strategies, adjoint method, hyperbolic equations
(14 pages, 2008

146. S. Desmettre, J. Gould, A. Szimayer
Own-company stockholding and work effort preferences of an unconstrained executive
Keywords: optimal portfolio choice, executive compensation
(33 pages, 2008)

147. M. Berger, M. Schröder, K.-H. Küfer
A constraint programming approach for the two-dimensional rectangular packing problem with orthogonal orientations
Keywords: rectangular packing, orthogonal orientations non-overlapping constraints, constraint propagation
(13 pages, 2008)

148. K. Schladitz, C. Redenbach, T. Sych, M. Godehardt
Microstructural characterisation of open foams using 3d images
Keywords: virtual material design, image analysis, open foams
(30 pages, 2008)

149. E. Fernández, J. Kalcsics, S. Nickel, R. Ríos-Mercado
A novel territory design model arising in the implementation of the WEEE-Directive
Keywords: heuristics, optimization, logistics, recycling
(28 pages, 2008)

150. H. Lang, J. Linn
Lagrangian field theory in space-time for geometrically exact Cosserat rods
Keywords: Cosserat rods, geometrically exact rods, small strain, large deformation, deformable bodies, Lagrangian field theory, variational calculus
(19 pages, 2009)

151. K. Dreßler, M. Speckert, R. Müller, Ch. Weber
Customer loads correlation in truck engineering
Keywords: Customer distribution, safety critical components, quantile estimation, Monte-Carlo methods
(11 pages, 2009)

152. H. Lang, K. Dreßler
An improved multiaxial stress-strain correction model for elastic FE postprocessing
Keywords: Jiang's model of elastoplasticity, stress-strain correction, parameter identification, automatic differentiation, least-squares optimization, Coleman-Li algorithm
(6 pages, 2009)

153. J. Kalcsics, S. Nickel, M. Schröder
A generic geometric approach to territory design and districting
Keywords: Territory design, districting, combinatorial optimization, heuristics, computational geometry
(32 pages, 2009)

154. Th. Fütterer, A. Klar, R. Wegener
An energy conserving numerical scheme for the dynamics of hyperelastic rods
Keywords: Cosserat rod, hyperealstic, energy conservation, finite differences
(16 pages, 2009)

155. A. Wiegmann, L. Cheng, E. Glatt, O. Iliev, S. Rief
Design of pleated filters by computer simulations
Keywords: Solid-gas separation, solid-liquid separation, pleated filter, design, simulation
(21 pages, 2009)

156. A. Klar, N. Marheineke, R. Wegener
Hierarchy of mathematical models for production processes of technical textiles
Keywords: Fiber-fluid interaction, slender-body theory, turbulence modeling, model reduction, stochastic differential equations, Fokker-Planck equation, asymptotic expansions, parameter identification
(21 pages, 2009)

157. E. Glatt, S. Rief, A. Wiegmann, M. Knefel, E. Wegenke
Structure and pressure drop of real and virtual metal wire meshes
Keywords: metal wire mesh, structure simulation, model calibration, CFD simulation, pressure loss
(7 pages, 2009)

158. S. Kruse, M. Müller
Pricing American call options under the assumption of stochastic dividends – An application of the Korn-Rogers model
Keywords: option pricing, American options, dividends, dividend discount model, Black-Scholes model
(22 pages, 2009)

159. H. Lang, J. Linn, M. Arnold
Multibody dynamics simulation of geometrically exact Cosserat rods
Keywords: flexible multibody dynamics, large deformations, finite rotations, constrained mechanical systems, structural dynamics
(20 pages, 2009)

160. P. Jung, S. Leyendecker, J. Linn, M. Ortiz
Discrete Lagrangian mechanics and geometrically exact Cosserat rods
Keywords: special Cosserat rods, Lagrangian mechanics, Noether's theorem, discrete mechanics, frame-indifference, holonomic constraints
(14 pages, 2009)

161. M. Burger, K. Dreßler, A. Marquardt, M. Speckert
Calculating invariant loads for system simulation in vehicle engineering
Keywords: iterative learning control, optimal control theory, differential algebraic equations(DAEs)
(18 pages, 2009)

162. M. Speckert, N. Ruf, K. Dreßler
Undesired drift of multibody models excited by measured accelerations or forces
Keywords: multibody simulation, full vehicle model, force-based simulation, drift due to noise
(19 pages, 2009)

163. A. Streit, K. Dreßler, M. Speckert, J. Lichter, T. Zenner, P. Bach
Anwendung statistischer Methoden zur Erstellung von Nutzungsprofilen für die Auslegung von Mobilbaggern
Keywords: Nutzungsvielfalt, Kundenbeanspruchung, Bemessungsgrundlagen
(13 pages, 2009)

164. I. Correia, S. Nickel, F. Saldanha-da-Gama
Anwendung statistischer Methoden zur Erstellung von Nutzungsprofilen für die Auslegung von Mobilbaggern
Keywords: Capacitated Hub Location, MIP formulations
(10 pages, 2009)

165. F. Yaneva, T. Grebe, A. Scherrer
An alternative view on global radiotherapy optimization problems
Keywords: radiotherapy planning, path-connected sublevelsets, modified gradient projection method, improving and feasible directions
(14 pages, 2009)

166. J. I. Serna, M. Monz, K.-H. Küfer, C. Thieke
Trade-off bounds and their effect in multi-criteria IMRT planning
Keywords: trade-off bounds, multi-criteria optimization, IMRT, Pareto surface
(15 pages, 2009)

167. W. Arne, N. Marheineke, A. Meister, R. Wegener
Numerical analysis of Cosserat rod and string models for viscous jets in rotational spinning processes
Keywords: Rotational spinning process, curved viscous fibers, asymptotic Cosserat models, boundary value problem, existence of numerical solutions
(18 pages, 2009)

168. T. Melo, S. Nickel, F. Saldanha-da-Gama
An LP-rounding heuristic to solve a multi-period facility relocation problem
Keywords: supply chain design, heuristic, linear programming, rounding
(37 pages, 2009)

169. I. Correia, S. Nickel, F. Saldanha-da-Gama
Single-allocation hub location problems with capacity choices
Keywords: hub location, capacity decisions, MILP formulations
(27 pages, 2009)

170. S. Acar, K. Natcheva-Acar
A guide on the implementation of the Heath-Jarrow-Morton Two-Factor Gaussian Short Rate Model (HJM-G2++)
Keywords: short rate model, two factor Gaussian, G2++, option pricing, calibration
(30 pages, 2009)

171. A. Szimayer, G. Dimitroff, S. Lorenz
A parsimonious multi-asset Heston model: calibration and derivative pricing
Keywords: Heston model, multi-asset, option pricing, calibration, correlation
(28 pages, 2009)

172. N. Marheineke, R. Wegener
Modeling and validation of a stochastic drag for fibers in turbulent flows
Keywords: fiber-fluid interactions, long slender fibers, turbulence modelling, aerodynamic drag, dimensional analysis, data interpolation, stochastic partial differential algebraic equation, numerical simulations, experimental validations
(19 pages, 2009)

Status quo: August 2009